SEDIMENTOLOGY
the journal of the
International Association of Sedimentologists

The influence of basin settings and flow properties on the dimensions of submarine lobe elements

Journal:	*Sedimentology*
Manuscript ID	SED-2019-OM-104.R1
Manuscript Type:	Original Manuscript
Date Submitted by the Author:	28-Jan-2020
Complete List of Authors:	Spychala, Yvonne; Universiteit Utrecht, Geosciences Eggenhuisen, Joris; Utrecht University, Earth Sciences Tilston, Mike; Universiteit Utrecht, Geosciences Pohl, Florian; Universiteit Utrecht, Geosciences
Keywords:	morphology, turbidity current, experimental study, dimensions, advection length, sand bias

The influence of basin settings and turbidity current flow properties on the dimensions of submarine lobe elements.

Spychala, Y.T.[1]*, Eggenhuisen, J.T.[1], Tilston, M.[1], Pohl, F.[1]

[1]EuroSEDS, Department of Earth Sciences, Utrecht University, 3584 CB Utrecht, NL

*Corresponding author: yts@gmx.de

ABSTRACT

Submarine lobes have been identified within various deep-water settings, including the basin-floor, the base of slope and the continental slope. Their dimensions and geometries are postulated to be controlled by the topographical configuration of the seabed, sediment supply system and slope maturitygradient. While confinement has been suggested as a main control factor for lobe dimensions, it does not explain the variationspread of lobe dimensions within individual systems.

Ten experiments were conducted in a 3D-flume to study the depositional characteristics of submarine lobes associated with 1) different basin floor dipping anglesgradients (0-4°), 2) different sediment concentration of the parent turbidity current (11-19 % Vol), and 3) varying discharge (25 - 40 m^3/h). Most runs produced lobate deposits that onlapped onto the lower slope. independent of basin floor dip and concentration. We determined that the deposits best describe the hierarchical level of lobe elements. Lobe elementDeposit length iwas proportional to basin-floor angle and sediment volume concentration. A higher amount of bypass is observed in the proximal area as the basin-floor angles get steeper and sediment concentrations higher. Deposits of runs with lower discharge could be traced higher upslope while runs with higher discharge produced an

area of low deposition behind the channel mouth, i.e. discharge controlleds whether lobe deposits awere attached or detached from their channel-levee systems. Integration of measured lobe element dimensions andA particle--advection--length- scale analysis shows suggests that this approachlatter can be used as a first order estimation of lobe element length. However, the estimations are strongly depended on the used average grain size used for calculations (e.g. silt is still actively transported after all sand has been deposited) and the method cannot be used to locate the main depocentre. Furthermore, attempted reconstructions of turbidity current velocities from natural systems suggest that the method is not appropriate for use in inversions fromon more complex composite bodies such as lobes.

Keywords: submarine lobesmorphology, turbidity current, experimental study. dimensions, advection length, sand biasvs. silt

INTRODUCTION

Submarine lobes are high aspect-ratio, sand-rich deposits fed by sediment gravity flows via channels. They are a major component of submarine fans, the largest depositional bodies on the planet, and therefore represent an important archive of palaeo-environmental change (e.g. Prélat et al., 2009; Flint et al.,2011; Romans et al., 2016). Submarine lobe deposits are also of economic interest because of their potential as hydrocarbon reservoirs. Thus, lobe characteristics such as dimensions, geometries, volumes and depositional sand quality are of high interest (e.g. Mulder and Alexander, 2001; Portén et al., 2016).

Traditionally, submarine lobe deposits were described as simple radial bodies that thin and become progressively finer-grained away from an apex (e.g. Normark, 1970; Mutti, 1977; Normark, 1978; Luthi, 1981; Lowe, 1982; Bouma, 2000). However, it has recently been recognized that the geometry of lobe deposits is more complicated (e.g. Nelson et al., 1992; Twichell et al., 1992; Gervais, 2006; Hodgson et al., 2006; Deptuck et al., 2008; Prélat et al., 2009; Etienne et al., 2012; Burgreen & Graham, 2014, Grundvåg et al., 2014, Spychala et al., 2017a). It has also been observed that lobe dimensions and aspect-ratios do vary significantly within individual submarine fans (Deptuck et al., 2008; Jegou et al., 2008; Saller et al., 2008; Prélat et al., 2009; Bourget et al., 2010; Morris et al, 2014; see Fig. 1). The cause of this variation in lobe dimensions ~~has not been studied yet, and is~~will be the focus of this paper. Prélat et al. (2010) proposed that, while lobe volumes have a narrow range, which is independent of the size of the overall deepwater system they are deposited in, lobe geometries and dimensions show strong influence from the local topography and the up-dip supply system. Confinement is seen as a main controlling factor in some publications, dividing systems in unconfined and confined lobes (Prélat et al., 2010), whereas Hamilton et al. (2017) ~~debate~~ spectulate that supercritical vs. subcritical behaviour connected to slope angles is the main control on lobe dimensions.

Outcrops and seismic datasets allow the in-depth study of lobe facies, internal architecture and plan-view geometries. ~~They do, however~~However, they do not allow for the direct study of the influence of controlling parameters of flow discharge, sand:mud ratio and basin set-up that led to the deposits (Posamentier and Kolla, 2003; Prélat et al. 2010). Laboratory experiments allow the manipulation of specific boundary conditions, and therefore their influence on the deposits can be directly quantified. In addition, instrumental documentation of changes to the flow can be conducted

systematically (e.g. Baas et al., 2004; Hamilton et al., 2017). While flume experiments traditionally focus on the behaviour of the flow itself, increasing effort has been invested to also model the development of prominent morphologies of submarine fans (e.g. Luthi, 1981; Ouchi et al., 1995; Parsons et al., 2002; Baas et al., 2004; Pyles et al., 2013; Fernandez et al., 2014; Hamilton et al., 2017, Steel et al., 2017, de Leeuw et al., 2018). Break in slope, channel dimensions, channel hydraulics, interstitial fluid density and grain-size distribution of the parent flow have been suggested to have an important influence on the architecture of lobes (Baas et al., 2004; Prélat et al., 2010, Cantelli et al., 2011, Fernandez et al., 2014; Hamilton et al., 2017, Steel et al., 2017, De Leeuw et al., 2018). Choi and Garcia (2001) have pointed out that longitudinal and lateral spreading of unconfined flows cannot be looked at in separation. i.e. the amount of lateral spreading governs how far a flow can spread longitudinally.

It is generally assumed that length of turbidity current deposits is primarily determined by the velocity of the flow, settling velocity of the particles and flow thickness (e.g. Mulder and Alexander, 2001; Lamb et al., 2010; Ganti et al., 2014). Ganti et al. (2014) suggested a simple mathematical approximation to determine the advection length (l_a) of a variety of sedimentary features, including submarine fans built up by turbidity currents. Advection length is defined as the horizontal length over which a characteristic particle is transported in the flow before it settles to the ground. This approach deals with three simple parameters: flow velocity (u), average settling height (h_s) and settling velocity of the characteristic particle size (w_s). Whether this advection length method can be used as a first order estimation tool for deposit geometry~~length~~ from turbidity currents~~,~~ is untested, while there are a number of issues that deserve scrutiny. For instance, if the basin slope is not fully horizontal but dipping at a gradient towards the basin, the gravitational pull must be expected to result in turbulence that

maintains suspension of the sediment beyond the advection length scale. We find previous considerations of the role of turbulence in advection length estimates to be too simplistic, and this will be discussed in detail later in this paper. Another process that could impact the length of transport on lobes is the concentration-dependence of the settling velocity, for instance through hindered settling (Richardson and Zaki, 1954). ~~or if other parameters like basin angle and turbulence intensity need to be incorporated, is untested.~~ ~~Using~~ Furthermore, ~~T~~the use of different grain sizes for calculations~~as characteristic particle will potentially~~can lead to very different estimated length scales, especially in mixed systems that are built by flows that comprise sand and silt grains. An interesting question to investigate is how a single advection length scale based on one characteristic grains size corelates to the areal distribution of facies associations in such mixed systems.

Silt-grained sediment is dominantly deposited in lobe fringe and distal lobe fringe environments in natural systems (Prélat et al., 2009; Etienne et al., 2012; Grundvåg et al., 2014; Marini et al., 2015; Spychala et al., 2017a,b) and was suggested to form a wide halo around the sandy lobe proportion as silt will still be transported basinwards and deposits long after the sand-sized grains have settled out. Nonetheless, deep-water studies primarily focus on the sand-prone deposits of submarine fans, creating a sand-prone bias and uncertainties about the real dimensions of deep-water lobes (Boulesteix et al., 2019).

Here, we systematically investigate the influence of basin morphology, volume concentration and discharge of the parent flow on lobe dimensions and geometries, while we keep grain-size distribution and channel morphology constant. Specific aims for the presented study are 1) to study the range of dimensions and geometries observed

from changing boundary conditions; 2) to investigate if observed depositional patterns can be related to flow properties; 3) to discuss which factors are controlling the differences in observed deposit shapes; 4) to debate if it is possible to predict dimensions and geometries from velocity (u) and settling velocity (w_s) alone, and, if yes, what are the caveats of this method? and, 5) to compare the discrepancy of predicted advection length using sand or silt particles as a characteristic parameter and discuss the role of silt-prone sediments as part of lobe deposits.

METHODS

Set-up and procedure

The experiments are conducted in the Eurotank Flume Laboratory at Utrecht University. The Eurotank is 6 m wide and 11 m long. The tank was filled up with water to a level of 1.2 m (Fig. 2A). The bathymetry created in the tank consisted of a 11° slope, a variable ~~dippinggradient~~ (0-4°) basin floor, and a horizontal termination at the end of the set-up that was used for setting up the measurement equipment (Fig. 2A). A channel (0.8 m wide and 0.05 m deep) with levees was built on the slope and restored to the same dimensions after each run. The channel dimensions are chosen to conform with the Run 4 presented in de Leeuw et al. (2018) They found that these channel dimensions resulted in only minor modification of the channel shape by erosion or deposition. This is desirable here because the focus of this paper is on lobe characteristics and channel evolution is ideally kept to a minimum. ~~equilibrium channel regime presented by Heijnen et al. (in prep.)~~. The entire set-up is covered by unconsolidated substrate with a similar composition to that used to generate the

turbidity currents (sand/ silt mixture with d50 of 133 µm) allowing for erosion by the incoming turbidity currents. Shields scaling (de Leeuw et al., 2016, Pohl et al., 2019~~in prep~~) was applied to create turbidity currents that allow for investigation of depositional processes.

The experimental series consist of ten runs in total; Runs 1-4 and 6 investigate the influence of the basin-floor gradient~~dip~~ (Series I), Runs 5-8 focus on the influence volume concentration of the sediment (Series II) and Runs 6,9 and 10 on different discharge (Series III). The values for each parameter in the individual runs are shown in Table 1. A mixture of sand and water (total volume: 0.9 m^3) with varying sediment volume concentrations (Series II) was prepared in a separate mixing tank. ~~The used sediment~~Sediment used is a mixture of 75% quartz grains (density: 2650 kg/m^3) and 25% ground glass (2500 kg/m^3) and has a median grain size (d50) of 133 µm. The mixture is pumped into the Eurotank using a radial flow pump. The discharge rate was set to 30 m^3/h for most of the runs except for the discharge series Run 9 and 10 (Table 1). The discharge was monitored with a discharge meter (Krohne Optiflux 2300). Experiments were run until the mixing tank was drained. Depending on the discharge this took between 80 and 100 seconds. The mixture then entereds the experimental set-up through an inlet box which has a 1 m section of non-erodible material attached to its front and gradually expanding side-walls. A small scour is generated where the flow passes onto the erodible section of the slope. As this erosion is an experimental artifact, it will be neglected in the evaluation of depositional and erosional patterns.

Data acquisition and processing

UVP

Velocity profiles of the turbidity currents were collected in four different locations (Fig.2B) using Ultrasonic Velocity Profiler probes (UVPs). The probes were set up 18 cm above the bed to prevent obstruction of the flow. They were oriented in a 60° angle to the local preformed bed. Bed-parallel velocity is calculated through trigonometry with the assumption that there is no average bed-perpendicular velocity and that the mean flow direction is in the vertical plane of the angled UVP beam. As the bed is the datum for the UVP data, and its position varies throughout the run due to erosion and deposition, the first step of the data processing phase involves identifying the temporal changes in bed position. Velocity profiles and flow thickness were averaged for individual runs for the body of the current. Velocity profiles and flow thicknesses for individual runs were averaged for the body of the flow by omitting the first 5 second (current head) and last 10 seconds (current tail) from the dataset ~~For time-averaged velocity profiles the start and end of the incoming current was picked with the first 5 seconds (current head) and last 10 seconds (current tail) omitted from the dataset. Bed-parallel velocity is calculated through trigonometry with the assumption that there is no average bed-perpendicular velocity and that the mean flow direction is in the vertical plane of the angled UVP beam.~~

DEM

Before and after each experiment a laser scan of the topography within the tank is conducted. These are used to create digital elevation models (DEMs) with a horizontal resolution of 2x2 mm and maps of the deposition and erosion that occurred during the runs. Changes in elevation less than 5 mm were omitted in the erosion/deposition maps to avoid interference of bed reworking (migration ripples) with depositional trends. After each experiment the dimensions (width, length, and thickness) of the lobe body

and its relation to the base of slope (detached or attached) were documented (Fig. 3), as well as the channel length and its ~~dip~~gradient. Width and length were measured with a tape measure in the tank and confirmed ~~by using~~in the DEMs, whereas thickness was established by looking at the longitudinal cross-sections created from the DEMs. Deposit lengths is defined as the length from the onset of deposition of the lobate deposit to its terminus. Strike-c~~C~~ross-sectional areas, which are a proxy for the depocentre, were determined by subtracting the DEMs of the initial topography from those of the post experimental topography.

Deposits are interpreted as attached if their onset o~~n~~f deposition is on the slope, whereas deposits that show distinctive thickening on the basin floor are interpreted as detached.

RESULTS

Morphology of lobe deposits

In this section, we present the dimensions and geometries of the deposits in detail in association ~~of~~ with the series they have been conducted in. A summary of the dimensions can be found in Table 2. Aside from the below described characteristic a~~A~~ll of the experimental deposits exhibit~~show~~ a ripple-field to the margins of the main sand body that is best developed to the frontal margin of the deposit ~~(Fig. 9)~~.

Series I: basin-floor slope

Run~~s~~ 1-4 and 6 (Series I) study the influence of the ~~dipping angle~~gradient of the basin floor on deposit~~lobe~~ dimensions and morphology. As the basin-floor angle increases from 0° to 4°, the length of the deposit~~lobe~~ increases from 310 cm to 383 cm, whereas

the width of the deposit~~lobe~~ decreases from 186 cm to 139 cm (Table 2 and Fig.4). This means that aspect ratios (L/W) vary from 1.7 to 3.2 (Table 2). While the maximum thickness only shows slight variations from 8.8 to 6.2 cm, the location of the thickest part of the deposit is situated distinctly farther from the break-of-slope as the basin-floor becomes steeper (Fig. 5). As the point of maximum thickness is located further downstream, more of the sediment volume also becomes progressively accumulated farther downstream, in effect relocating the depocentre out onto the basin floor (Fig. 6A). All deposits have prominent lobate cross-sections. The exception is Run 6 which shows a small indent (1 cm) to the generally convex top of the deposit in the proximal area ~~(Fig. 6A)~~, for the first 50 cm~~,~~ after the break-of-slope (Fig. 8A). All deposits, except the one formed by Run 1, onlap onto the slope (Fig. 5).

Series II: sediment volume concentration

Runs 5-8 (Series II) investigate the effect of varying sediment concentration. ~~It can be observed~~ Results indicate that deposit length is proportional to concentration (Figs. 5C and 8), i.e. the run with the highest sediment concentration (Run 5; 19% Vol) is the longest (465 cm), whereas the run with the lowest concentration (Run 8; 13% Vol) is the shortest (340 cm). Deposits of Run 6 (17% Vol) and Run 7 (15% Vol) are 444 cm and 390 cm long, respectively (Fig. 9). Width dimensions do not show much variability (Table 2) ranging from 143 cm to 139 cm. It is worth noting that Run 8, which has the lowest sediment concentration, has a narrower width of 123 cm~~, though~~. Aspect ratios (L/W) range from 2.7 to 3.4 (Table 2) which means that these deposits are highly elongated. Maximum thickness values show a clear decrease with lower sediment concentrations of the flow (Fig. 5). While a flow with 19% Vol has a deposit with the maximum thickness of 7.8 cm, a flow of 13% Vol has a deposit with a maximum

thickness of 5.6 cm. In Series II, two distributions of sediment volume can be observed (Fig. 6B). The runs with the higher concentration (Run 5 and 6) have most of their sediment volume deposited in the intermediate to distal part of the deposit~~lobe,~~ while the runs with lower sediment concentration (Run 7 and 8) have most of their volume deposited in the proximal area. Cross-sections show small indents to the convex tops of the deposit for Run 5 and 6 (between 0.5 and 1 cm; up to 1.5 m from the break-of-slope), while Run 7 and 8 show prominent convex lobe geometries throughout the deposit (Fig. 8B). All runs of Series II ~~show~~ onlap onto the slope. Deposition in the channel becomes more prominent with decreasing sediment concentration of the flow.

Series III: Discharge

~~Finally,~~ Runs 6, 9 and 10 (Series III) were conducted to examine the consequence of changing discharge to the dimensions of the resulting deposits. There is no observable trend in the length of the deposits associated with higher or lower discharge, in fact a discharge of 30m^3/h (Run 6) produces a slightly longer deposit~~lobe~~ (444 cm) than a discharge of 40m^3/h (Run 10; 430 m). The same is true for the width of the deposits (Table 2), that vary between 143 and 118 cm, and maximum thickness that ~~show a~~ range from 5.6 to 6.9 cm (Fig. 5), but show no correlation to discharge changes. Aspect ratios (L/W) range from 3.1 to 3.4 (Table 2). The main depocentres for the resulting deposits are located in an intermediate to distal position, with the exception of Run 9 (lowest discharge; 25m^3/h) that has more longitudinal uniformity in its depositional thickness (Fig. 6C). The main difference between the three runs is the point of onset of ~~lobe~~ deposition (Fig. 9). This point is located further down-dip with higher discharges. While the deposit of Run 9 onlaps high up on the slope (after 190 cm of slope length) shortening the total slope length, the deposit of Run 6 onlaps at 210 cm at the base of

the slope, and the deposit of Run 10 is detached from the slope (250 cm from the inlet). An area of low deposition is located between the break-of-slope and the deposit~~lobe~~ for Run 10 (Fig. 9). ~~It~~ The deposit shows irregular geometries for 2 m after the break of slope before the deposit thickens and ~~shows~~ develops a convex geometry in cross-section. Deposits of Run 9 fill the channel form upslope, while deposition from Run 6 and 10 drape the channel form while keeping it with the same dimensions although slightly shallower (4.5 cm instead of 5 cm depth).

~~All of the experimental deposits show a ripple field to the margins of the main sand body that is best developed to the frontal margin of the deposit (Fig. 9).~~

Flow properties

Flow velocities

At the break of slope the average velocity for the runs of Series I (Runs 1,2,3,4 and 6) varies from 0.64 m/s to 0.53 m/s with no observable trends in association with change in the downstream basin floor angle (Fig.10A). However, at the position of UVP 7 (Fig. 2B) a pattern starts to develop: Run 6 which corresponds with the steepest basin floor (4°) maintains velocities of 0.34 m/s, whereas the maximum velocity decreases more abruptly with shallower basin-floor gradients and most with a horizontal basin floor (0.2 m/s).

For runs with changing concentration (Series II; Fig. 10B) it can be stated that runs with higher sediment volume concentration (Run 5 and 6) show slightly higher channel exit velocities (0.62 m/s and 0.63 m/s) than those with lower sediment volume concentrations (Run 7: 0.61 m/s; Run 8: 0.54 m/s). The trend becomes more prominent downstream, and velocities correlate positively with sediment concentration at the locations of UVP probes 6 and7. A similar trend can be observed in Series III (Fig.

10C), where runs with higher discharge ~~show~~ have higher initial maximum velocities at the break of slope where the flow experiences the loss of confinement and a lower velocity decay rate.

Flow thickness

Flow thickness doesn't show any clear trends for Series I and III (Fig. 10). In Series II it could be observed that runs with lower sediment volume concentrations (Run 7 and 8) have lower initial flow thicknesses and may thicken downstream (Run 8), while runs with higher sediment volume concentration (Run 5 and 6) are thicker on the break of slope and gradually thinner downstream.

DISCUSSION

Controlling factors of lobe length and geometries

The runs of Series I suggest~~show~~ that ~~lobe element~~ deposits get subsequently longer, narrower and thinner when the basin-floor angle is increased. This is due to slower loss of streamwise velocity as gravity forces acting on the current counteract its deceleration through loss of excessive density as the flow deposits sediment. There is a lag time until the current adjusts to the new conditions on the basin floor (Mulder and Alexander, 2001) therefore the correlation in flow deceleration with basin-floor angle can best be observed in UVP 7 (Fig. 10A). The deposit of Run 1 detached from the slope as sediment suspension is enhanced as energy from downslope travel needs to be dissipated at this abrupt break in slope (11°; e.g. Mulder and Alexander, 2001; Gray et al., 2005), ~~depositing the grains~~Following this enhanced suspension, grains deposit according to flow velocity and settling velocity, i.e. the faster the flow the further

detached the lobe deposit ~~(e.g. Mulder and Alexander, 2001; Gray et al., 2005)~~. Successively the current loses its capacity to carry the bulk of its sediment on the horizontal basin floor, and becomes strongly depletive (Cantero et al., 2014; Eggenhuisen et al., 2017). In contrast to this scenario, basin floor angles that are more inclined enable sediment to be bypassed more efficiently through~~out~~ the basin, eventually relocating the depocentre of the lobe element (Run 6; Fig. 6A).

The outcome of Series II indicates~~shows~~ that changing volume concentration primarily controls ~~lobe element~~deposit length and the position of the depocentre, while ~~lobe~~ deposit width does not seem to be much influenced. This conforms with observations made on enhanced transport efficiency associated with higher initial densities (Laval et al., 1988; Gladstone et al., 1998; Al Ja'Aidi et al., 2004). The extension of deposition further into the basin can be explained with two mechanisms. Firstly, –h~~H~~igher concentration runs have higher initial velocities at the break of slope compared to low concentration runs due to more excess density (Run 8 vs. Run 5; Fig. 10B), i.e. their driving force is larger~~bigger~~. ~~This conforms with observations made on enhanced flow efficiency associated with higher initial densities (Laval et al., 1988; Gladstone et al., 1998; Al Ja'Aidi et al., 2004).~~ Additionally, higher concentration runs ~~show~~ exhibit ~~slower~~ less velocity-loss ~~downstream~~ as they travel over the basin floor, because~~as~~ the overall sediment concentration of the current throughout remains higher compared to low concentration runs. The elongated geometry of the deposit and volume distribution of higher concentration flows suggest that the sediment concentration has reached a limit where hindered settling (Richardson and Zaki, 1954) has at least a partial influence (Kneller and Branney, 1995). Hindered settling refers to the decrease in settling velocity of particles due to the interaction with other particles in the fluid. Decreased settling velocities cause the sediment to be advected farther into the basin before it settles. Also,

indents in the convex tops of the lobate deposits (Run 5 and Run 6; Fig. 8A) point to an increased bypass rate in the proximal axial area of the deposits which explains the relocation of the ~~lobe element~~ depocenter farther downstream. These indent morphologies may be (a precursor of) distributary lobe-top channels (see Jegou et al., 2008). It remains to be tested if they represent long-term conduits (Mutti and Normark, 1987) or if they will be filled in by the next incoming event.

Series III suggests~~shows~~ that changing discharge does not affect the length of the ~~lobe elements~~deposits significantly, but steers whether the deposits are attached or detached from the slope. As higher discharge runs have higher velocities (Fig. 10) they have a higher capacity to transport sediment past the break of slope. Run 10 with the highest discharge transports the sediment farthest out into the basin producing the most elongated lobe element deposit (L/W: 3.4).

In summary, sediment suspension is maintained fa~~u~~rther into the basin by ~~higher~~ steeper basin-floor slope, higher flow discharge, and higher sediment concentrations. The effect on the dimensions of the ~~lobe~~ deposit differ, though: increased slope changes the planform dimensions, increased sediment volume concentration moves the depocenter fa~~u~~rther into the basin, and increased discharge controls the point of onset of deposition ~~onset~~ , while leaving the ~~lobe~~ deposit dimensions more or less the same.

Level of hierarchy

When comparing experimental data to field data the proper level of hierarchy has to be established (cf. Hamilton et al., 2017) to make useful statements. We recognise that a lobe is a composite body comprised of predominantly compensational stacked lobe elements, that are themselves built of several beds (Deptuck et al., 2008; Prélat et al., 2009; Mulder & Etienne, 2010; Prélat et al., 2010; Bernhard et al., 2012; Etienne et al.,

2012; Grundvåg et al., 2014; Marini et al., 2015; Picot et al., 2016; Zhang et al., 2016; Spychala et al., 2017a,b; see Fig. 11). This complexity cannot be modelled by single flow--event experiments. However, it is documented that strength of compensation decreases with lower hierarchical levels (Straub and Pyles,et al., 2012), as bed-scale stacking is laterally constrained by the genetically related channel resulting in more or less aggradationally stacked beds that form lobe elements (Fig. 11). This means that small hierarchicalal units like lobe elements form by weakly compensational stacked beds and their dimensions will ultimately be similar to those of their building blocks (beds). The fact that it is possible to interpret lobe elements in the field through the facies similarity of the beds that form them (e.g. Prélat et al., 2009; Prélat and Hodgson, 2013) further strengthens the assumption that the depositional areafield has stayed relatively stable during their sedimentation. Therefore, we suggest that observations made during in oursingle experimental flows experiments on single flows can also be used to compare against lobe element geometriesbodies.

Lobe dimensions in natural systems

Prélat et al. (2010) suggested that confinement is the main force behind the division of thick and areally small, and thin, but areally extensive, lobe deposits. This was already debated by Hamilton et al. (2017), who stateding that higher slope angles can produce thicker lobes relative to their area without the need of confinement. Our experiments confirm this finding somewhat for lobe elements, although we show that the basin-floor angle does play as important a role as the slope angle. This suggests that lobe element deposited in relatively steep dipping intraslope basins (e.g. Prather et al., 1998; Adeogba et al., 2005; Gamberi and Rovere, 2011; Barton et al., 2012; Pirmez et al., 2012) have different geometries from lobe elements deposited on nearly horizontalthe

399 ~~relatively gentle dipping~~ basin floors. However, lobes are composite bodies formed by
400 several lobe elements creating significantly larger deposits. It is to be expected that
401 confinement has an influence on lobe element stacking patterns (aggradational vs.
402 compensational stacking), which will determine if the lobe body itself is thick and
403 areally small, or thin and areally wide. Therefore, confinement cannot be dismissed as
404 an important factor on the composite lobe bodies.
405 Increased sediment supply (sediment volume concentration and/or sediment discharge)
406 to the basin, whether as a response to relative sea-level fall and/or progressive
407 confinement and increase of turbidity current efficiency (Mutti, 1992; Gardner et al.,
408 2003; Kneller, 2003; Hodgson et al., 2016), is thought to steer progradation of the
409 turbidite system into the basin. Our experiments conform to this model~~ such as~~ runs
410 with the highest sediment volume concentration and highest discharge (Run 5 and Run
411 10) are able to bypass more sediment basinwards. Increased bypass is marked either by
412 an indent in the lobe element top or an area of relative low sedimentation rate that
413 effectively detaches the lobe element deposit from the slope. In contrast, runs with low
414 sediment concentration and discharge (Runs 8 and 9) may represent lobe elements
415 formed during waning sediment supply to the basin through raising relative sea-level
416 and/or channel system aggradation and widening.
417 This suggests that lobe deposits formed during low vs. high sediment supply may
418 haveshow distinctive ~~different geometries in their~~ morphologiesy as well as~~ their~~
419 relations with the channelized slope, raising the question if the erosive channel-lobe
420 transition zone (e.g. Palanques et al., 1995; Wynn et al, 2002; Hofstra et al., 2015, Pohl
421 et al., 2019) is a transient feature and therefore rarely observed in ancient outcrops (cf.
422 Brooks et al., 2018).
423

Can we estimate lobe element dimensions with simple mathematical assumptions?

Advection length, which is defined as the horizontal length of over which a characteristic particle is transported in the flow before it is deposited, has been proposed as a simple method to establish length scales of turbidity current deposits (Mulder and Alexander, 2001; Lamb et al., 2010; Ganti et al., 2014). It deals with three parameters only: flow velocity (u, in m/s), ~~average~~ settling height (h_s, in m) and settling velocity (w_s, in m/s). Advection length of a sediment particle (l_a, in m) is defined as:

$$l_a = u h_s / w_s \quad (1)$$

~~To test if the advection length approach leads to good estimations on lobe element length scales, we~~ We compare measured results from our experimental runs with calculated~~estimated~~ advection length values to test if the advection length approach leads to ~~good~~accurate first order estimations on lobe element length scales. To this end we use the average velocities reported from UVP 4 at the break of slope where the currents enter the unconfined basin floor and start spreading and depositing. ~~As turbidity currents are density stratified (Kneller and Branney, 1995; Sohn, 1997; Amy et al., 2005, Cartigny et al., 2013; Cantero et al., 2014; Tilston et al., 2015), we cannot assume a homogeneous sediment concentration profile. Thus, we corrected the settling height for the currents' near-bed concentration:~~

~~$h_s = h/r_o$ (2)~~

~~with r_o = near bed concentration (%)/ initial concentration (%) (Ganti et al.,2014). Near-bed concentration data were taken from separate 2D experiments (Pohl et al., in review) for 17% sediment volume concentrations.~~ Ganti et al. (2014) propose to use an average settling elevation as the characteristic vertical scale. This takes into account the density stratification of turbidity currents (Kneller and Branney, 1995; Sohn, 1997; Amy et al., 2005, Cartigny et al., 2013; Cantero et al., 2014; Tilston et al., 2015), which causes the

majority of sediment to be suspended low in the flow. However, in our analysis we are initially interested in predicting the length scale of the lobe elements, which is set by settling of advected particles that were initially at the top of the flow. We therefore choose the flow thickness as the relevant vertical length scale. Finally, we used the d_{50} of the initial suspension (d_{50}= 133µm) as the characteristic grain size. The settling velocity for this grainsize was calculated to be 1.23 cm/s (Ferguson and Church, 2004). All calculated advection lengths and measured ~~lobe element~~deposit lengths as well as used parameters can be found in Table 3.

Generally, ~~predicted~~ calculated lengths are ~~more than 50~~around 75 % accurate compared to measured deposit lengths (Table 3; Fig. 12), with the exception of the calculated advection lengths of Run 1, which will be discussed separately below. This means that advection length can be used as a first order estimation of lobe element length, although length values are consistently under predicted (Fig.12). We propose that this under prediction is due to several factors. ~~the fact that~~Firstly, the equation does not account for the effect of turbulence in turbidity currents (Middleton and Hampton, 1973; Southard and Mackintosh, 1981; Kneller and Buckee, 2000; Shringapure et al., 2012) and secondly, the result strongly depends on the chosen grain size and representative settling height used for calculation.

Settling is counteracted by turbulent mixing, and grains will therefore remain in suspension longer in the presence of turbulence~~before they settle to the bed.~~ This effect does not rely on an-isotropy of turbulent statistics (cf. Ganti et al. 2014), but on positive correlation between velocity and concentration fluctuations: upwards moving patches of fluid advect higher sediment concentrations upwards, while downwards moving patches of fluid advect lower sediment concentrations downwards. These correlated

fluctuations average out to an upwards positive flux of sediment that works against the settling of sediment (e.g. Garcia, 2008). In a steady flow that bypasses all of its sediment (*sensu* Stevenson et al., 2015), the settling flux is entirely balanced by the turbulent advection flux. In a depletive, but still turbulent turbidity current, the turbulent advection flux partially counteracts settling, and it is thus expected to delay deposition and carry sediment beyond the distances predicted by the advection length. The advection length resulted in the most accurate prediction for Run 1 ~~and Run 5~~ (102~~70~~ % accurate; Fig. 12). The turbidity current in Run 1 ~~this experiment~~ travelled onto a horizontal basin-floor, and became highly depletive after passing the break of slope. ~~It worked worst for Run 8 (48% accurate; Fig. 12), probably because near-bed concentrations are estimated too high and therefore the corrected settling height is too low.~~ We conclude that the advection length as estimated from the turbidity current structure at the break of slope is a very accurate approximation of lobe element length in situations where the flows are highly depletive and deposition starts on the basin floor. ~~In general, f~~Factors that ~~sedimentation~~increase the efficiency of sediment transport into the basin (*sensu* Mutti and Normark, 1987)~~disturb the patterns of high depletive sedimentation~~, such as steeper basin floor-angles, and higher sediment concentration and discharge, lead to less accurate ~~length~~ underpredictions of lobe element length.

A note should be made regarding the use of a constant advection velocity to estimate the advection length scale. Turbidity currents slow down while they flow over lobes and deposit their sediment. The flow velocities were generally decreased to 62-34% at the distal edge of the sandy deposits when compared to the velocity at the location of UVP4. A more complicated advection settling model would account for this decrease in advection velocity, which would result in further under-prediction of lobe element

length. This indicates that the efficiency effects described above are likely even more significant than indicated by the appearance of data in Table 3 and Figure 12.

Length estimations with the advection length approach have to be carried out keeping in mind that the final result is strongly linked to the used "characteristic" grain size and representative height (Fig. 13A). For example, in this case we have used a d_{50} of 133 µm (fine sand) biasing our result to the sand grains in our currents. The effect on estimated lobe element dimensions by omitting silt particles is discussed below. In addition, although advection length is useful to predict dimensions for specific grain sizes, it is still important to have a firm understanding of the overall deposit geometry to pinpoint the main depocentre and its relation to the slope (attached vs. detached.) The principles behind advection length (a simple settling from a stratified flow, with lowest and coarsest grains settling fastest) suggests a simple tapering wedge shape for the created deposit with the main depocentre located proximal to the break of slope. However, basin-floor slope, high concentration, and high discharge shift the depocentre farther basinwards. Figure 13B illustrates how the calculated length of the deposit of Run 10 does not only underestimate the dimensions, but also poorly characterises the depocentre position of the lobe element.

Can we use advection length to reconstruct turbidity current velocities from natural systems?

Advection length is a simple method to estimate first order length scale for the deposits resulting from our experiments. The corollary of successful prediction is that the method can also be used for inversion modelling. The question thatus arises whetheris if we could also use this method to give us an idea of the velocities of typical turbidity

currents ~~velocities~~ that have deposited natural systems. The data chosen to test this encompass four systems whose lobe dimensions, grain sizes and channel depth close to the channel-lobe transition zone were reported. Channel depth values were taken as an estimation for the flow height. Care was taken to ensure ~~used~~ lobe dimensions used conform to the same hierarchical level. The datasets chosen include the Amazon Fan (Jegou et al., 2008), Fan 3, Tanqua depocentre, Karoo Basin (Prélat et al., 2009, Kane et al., 2017), the Golo Fan offshore Corsica (Deptuck et al., 2008; Hamilton et al., 2017) and the Pleistocene Fan, Kutai Basin, Indonesia (Saller et al., 2004, 2008). Table 4 shows all calculated velocities for these four systems.

With the exception of the reconstructed velocities from the Pleistocene Fan of the Kutai Basin (1.75 – 9.1 m/s) all the calculated values reconstructed from lobe measurements are deemed far too high (> 10 m/s) to be sensible in respect to other measured (0.4- 3.5 m/s depth-average flow velocity; Khripounoff et al., 2004; Cooper et al., 2012; Liu et al., 2012; Xu et al., 2014) and estimated (–3.8 m/s depth-average flow velocity; Stevenson et al., 2018) turbidity current velocities from natural systems that are not caused by major earthquakes (up to 20 m/s; see Talling et al., 2013). However, using lobe element dimension from Fan 3 of the Karoo Basin instead of lobe dimensions, a much more reasonable value of 4.2 m/s for the current velocity is estimated, although this is still somewhat high (Table 4). Our experiments taught us, that advection length is in average about 75% accurate. With that in mind calculated velocities are likely to be too high even on the lobe element scale.

~~This outcome~~Still, the fact that calculated velocities for lobe elements seem more reasonable than for lobes underlines anew the composite nature of lobe deposits that is a sum of their lobe element dimensions and stacking patterns which are in turn affected by the properties of incoming turbidity currents, their modification through the channel

fairways and underlying topography. A lobe formed by progradational stacked lobe elements would for example result in overestimated flow velocities with this approach due to the successive basinward change of the transition from channel to lobe element as sediment is bypassed through the development of distributive channels that extend farther into the basin ~~(Fig. 15)(see Ferguson et al. in review)~~. On the other hand, lobe elements that are aggradationally stacked to form a lobe will give more reasonable estimations of current velocities. In addition, the maintenance of suspension into the basin through basin setting and sediment concentration of the turbidity current are other important factors that need to be taken into account as they can cause hindered settling and/or progradation into the basin. ~~Our experiments taught us, that advection length is in average about 50% accurate. With that in mind calculated velocities are likely to be two times to high even on the lobe element scale. For the Karoo in particular this would result in velocities of 2.1 m/s, which are reasonable numbers for a system that has been continuously built up.~~

Depositional trends sand vs. silt

~~Silt-grained sediment is dominantly deposited in lobe fringe and distal lobe fringe environments (Prélat et al., 2009; Etienne et al., 2012; Grundvåg et al., 2014; Marini et al., 2015; Spychala et al., 2017a,b) and was suggested to form a wide halo around the sandy lobe proportion as silt will still be transported basinwards and deposits long after the sand-sized grains have settled out. Lack of exposure, insufficient seismic resolution, and bias towards sand-prone lobe deposits have impeded the estimation of length scales of these silt-prone deposits to be established, although they can create features of 100 meters thickness when lobe deposition experiences lateral confinement (cf.~~

~~aggradational lobe fringes, Spychala et al., 2017b).~~ Lack of exposure, insufficient seismic resolution, and bias towards sand-prone lobe deposits have impeded the estimation of length scales of the silt-prone deposits of the lobe distal fringes to be established, although they can create features of 100 meters thickness when lobe deposition experiences lateral confinement (cf. aggradational lobe fringes, Spychala et al., 2017b;Boulesteix et al., 2019). Our experiments enable us to give first quantitative ~~predictions~~ assumptions on the distance silty material is transported and deposited after all sand has been deposited from the flow.

For Run 8 UVP 7 captures the transition from sand-prone deposits to silt-prone deposits. Average velocities at this point are still at 0.24 m /s. Settling velocities of silt sized grains are much smaller that for the sand (0.0014 m/s vs. 0.014 m/s). If we use the simple advection length method we can estimate~~show~~ that silt will be deposited for another 9.2 m (see Table 3) in a longitudinal direction, effectively changing lobe element length from 3.4 m to 12.6 m.

Consequently, we have to start thinking of lobes in a different way than before. The sand-prone part (lobe axis and off-axis environments) of a lobe only covers a small proximal portion of the whole deposit (Fig. 14) and transitions laterally into heterolithic packages that form the lobe fringes. The dimensions of the lobe fringes are governed by the variations in dimensions and the manner of stacking between beds and lobe elements. Finally, silt-prone distal fringes are the most areally widespread parts of lobes (Fig. 14). This results further strengthens the argument that several metres-thick siltstone intervals named “lobe fringe complexes” or “interlobes” (Prélat and Hodsgon, 2013; Spychala et al., 2017a) separating lobe complexes are formed by autogenic processes (Prélat et al., 2009; Spychala et al., 2017a, Boulesteix et al., 2019) instead of genetical unrelated sedimentation (Satur et al., 2000; Johnson et al., 2001; Van der

Werff and Johnson, 2003; Hodgson et al., 2006; Mulder and Etienne, 2010; McArthur et al., 2017), and may be traced laterally or up-dip into sand-prone lobe complexes that are located up to several kilometers away. In fact, Boulesteix et al. (2019) show that distal lobe fringes of Fan 3 of the Skoorsteenberg Fm. (Karoo Basin, SA) extended more than 18 km beyond the sand-stone pinchout.

CONCLUSIONS

Ten experimental runs where performed to test the influence of basin geometry, sediment volume concentration and discharge on lobe element dimensions and the architecture of their depositional bodies. ~~We suggesthow that~~The experimental lobe element length is proportional to basin-floor angle and sediment volume concentration, whereas discharge is the main ~~control~~ factor controlling~~on~~ the onset of lobe element deposition. Higher amounts of bypass behind the break of slope are observed with steeper basin-floor angles, higher concentration and higher discharge. Future research should aim to cover multiple successive runs to test how these initially formed depositional bodies develop over time. Flow properties show only subtle differences.

Our results suggest that lobe element deposits formed during different stages of the sediment supply cycle have pertinent different geometries~~.~~ We tested the ~~option to~~accuracy of ~~-~~estimate~~e~~ing lobe element dimensions with ~~the~~ simple ~~mathematical approach of~~ advection length calculations. On a first order this method gives a good prediction of the length of lobe element deposits created in our experiments. However, a consistent under prediction of length scales is observed, because maintenance of sediment suspension into the basin through either turbulence production (basin floor slope and flow discharge)~~, and hindered settling (sediment concentration)~~ is neglected. Attempts to reconstruct turbidity current velocities that have deposited natural systems

additionally indicate~~show~~, that this approach is hierarchy dependent and cannot be expected to yield reasonable results for higher order composite sedimentary bodies, such as lobes and lobe complexes, that are built by a multitude of turbidity currents over an extended period of time.

Finally, we established that reconstructions of lobe geometries are biased towards their sandy parts, even though silt-prone deposits are still deposited long after all the sand grains have been depleted. This is partly due to missing outcrop exposures, seismic resolution, and partly due to a general bias to sand-prone lobe deposits. This outcome strengthens the interpretation of silt-prone intervals (termed distal lobe fringes or intralobes) to be formed by autogenic process of lobe deposition rather than representing background sedimentation.

ACKNOWLEDGEMENTS

This project was funded by NWO (grant #NWO-ALW-Vidi-864.13.006), ExxonMobil, Shell and Equinor~~Statoil~~ for which we are thankful. Thony van der Gon-Netscher and Han de Witte supplied technical support to the experimental work. Reviews by Sedimentology Associate Editor Kyle Straub and reviewer Elisabeth Steel greatly improved the manuscript.

REFERENCES

Adeogba, A.A., McHargue, T.R. and **Graham, S.A.** (2005). Transient fan architecture and depositional controls from near-surface 3-D seismic data, Niger Delta continental slope. *AAPG Bulletin* **89**, 627-643.

Al Ja'aidi, O.S., McCaffrey, W.D. and **Kneller, B.C.** (2004). Factors influencing the deposit geometry of experimental turbidity currents: implications for sand-body architecture in confined basins. In: *Confined Turbidite Systems* (Eds S.A. Lomas and P. Joseph). Geological Society, London*, Spec. Publ.*, 222, 45-58.

Amy, L.A., Hogg, A.J., Peakall, J. and **Talling, P.J.** (2005). Abrupt transitions in gravity currents. *J.Geophys. Res.* **110**, F03001.

Baas, J.H., Van Kesteren, W. and **Postma, G.** (2004). Deposits of depletive high-density turbidity currents: a flume analogue of bed geometry, structure and texture. *Sedimentology* **51**, 1053-1088.

Barton, M.D. (2012). Evolution of an Intra-Slope Apron, Offshore Niger Delta Slope: Impact of step geometry on apron architecture. In: *Application of the principles of seismic geomorphology to continental -slope and base-of-slope systems: Case studies from seafloor and near-seafloor analogues* (Eds. B.E. Prather, M.E. Deptuck, D. Mohrig, B. van Hoorn and R.B. Wynn), *SEPM Spec. Publ.,* 99, 181- 197.

Bouma, A.H. (2000). Fine-grained, mud-rich turbidite systems: Model and comparison with coarse-grained, sand-rich systems. In: *Fine-grained Turbidite Systems* (Eds. A.H. Bouma and C.G. Stone) *AAPG Memoir 72/SEPM Spec. Publ.,* 68, 9-19.

Boulesteix, Kévin, Miquel Poyatos-Moré, Stephen Flint, David M. Hodgson, Kevin G. Taylor, and **Gareth R. Parry.** (2019). Sedimentary Facies and Stratigraphic

673 Architecture of Deep-water Mudstones Beyond the Basin-floor Fan Sandstone
674 Pinchout. *EarthArXiv*. July 9. doi:10.31223/osf.io/3qrew

675

676 **Brooks, H.L., Hodgson, D.M., Brunt, R.L., Peakall, J., Hofstra, M.** and **Flint, S.S.**
677 (2018). Deep-water channel-lobe transition zone dynamics: Processes and depositional
678 architecture, an example from the Karoo Basin, South Africa. *Geol. Soc. Am. Bull.,* **130**,
679 1723-1746.

680

681 **Burgreen, B.** and **Graham, S.** (2014). Evolution of a deep-water lobe system in the
682 Neogene trench-slope setting of the East Coast Basin, New Zealand: Lobe stratigraphy
683 and architecture in a weakly confined basin configuration. *Mar. Petrol. Geol.,* **54**, 1-22.

684

685 **Bourget, J., Zaragosi, S., Mulder, T., Schneider, J.-L., Garlan, T., Van Toer, A.,**
686 **Mas, V.** and **Ellouz-Zimmermann, N.** (2010). Hyperpycnal-fed turbidite lobe
687 architecture and recent sedimentary processes: Acase study from the Al Batha turbidite
688 system, Oman margin. *Sed. Geol.,* **229**, 144-159.

689

690 **Cantelli, A., Pirmez, C., Johnson, S.** and **Parker, G.** (2011). Morphodynamic and
691 Stratigraphic Evolution of Self-Channelized Subaqueous Fans Emplaced by Turbidity
692 Currents. *J. Sed. Res*., **81**, 233-247.

693

694 **Cantero, M., Balachandar, S., Cantelli, A.** and **Parker, G.** (2014). A simplified
695 approach to address turbulence modulation in turbidity currents as a response to slope
696 breaks and loss of lateral confinement. Environment Fluid Mechanics, **14**, 371-385.

697

Cartigny, M., J.B., Eggenhuisen, J.T., Hansen, E.W.M. and **Postma, G.** (2013). Concentration-Dependent Flow Stratification In Experimental High-Density Turbidity Currents and Their Relevance To Turbidite Facies Models. *J. Sed. Res*., **83**, 1047-1065.

Choi, S.-U. and **Garcia, M.H.** (2003). Spreading of Gravity Plumes on an Incline. *Coastal Engineering Journal*, **43:4**, 221-237,

Cooper, C., Wood, J. and **Andrieux, A.** (2013). Turbidity current measurements in the Congo Canyon, OTC Abstract 23992. Offshore Technology Conference, 6–9 May, Houston, Texas 12 pp.

de Leeuw, J., Eggenhuisen, J.T. and **Cartigny, M.J.B.** (2016). Morphodynamics of submarine channel inception revealed by new experimental approach. *Nature Comm*., **7**, Article number: 10886.

de Leeuw, J., Eggenhuisen, J.T., Spychala., Y.T., Heijnen, M.S., Pohl, F. and **Cartigny, M.J.B**. (2018). Sediment Volume and Grain-Size Partitioning between Submarine Channel-Levee Systems and Lobes: An Experimental Study. *J. Sed. Res*., **88**, 1-18.

Deptuck, M.E., Piper, D.J.W., Savoye, B. and **Gervais, A.** (2008). Dimensions and architecture of late Pleistocene submarine lobes off the northern margin of East Corsica. *Sedimentology*, **55**, 869-898.

Etienne, S., Mulder, T., Bez, M., Desaubliaux, G., Kwasniewski, A., Parize, O., Dujoncquoy, E. and **Salles, T.** (2012). Multiple scale characterization of sand-rich distal lobe deposit variability: Examples from the Annot Sandstones Formation, Eocene–Oligocene, SE France. *Sed. Geol.*, *273*, 274, 1-18.

~~**Ferguson, R.A., Kane, I.A., Eggehuisen, J.T., Pohl, F., Tilston, M., Spychala, Y.T.** and **Brunt, R.L.** (in review). Disentangling external and internal controls on submarine fan evolution.~~

Fernandez, R.L., Cantelli, A., Pirmez, C., Sequeiros, O. and **Parker, G.** (2014). Growth patterns of subaqueous depositional channel lobe systems developed over a basement with a down-dip break in slope: Laboratory experiments. J. Sed. Res., **84**, 168-182.

Flint, S.S., Hodgson, D.M., Sprague, A.R., Brunt, R.L., van der Merwe, W.C., Figueiredo, J., Prélat, A., Box, D., Di Celma, C. and **Kavanagh, J.P.** (2011). Depositional architecture and sequence stratigraphy of the Karoo basin floor to shelf edge succession, Laingsburg depocentre, South Africa. *Mar. Petrol. Geol.*, 28, 658-674.

Gamberi, F. and **Rovere, M.** (2011). Architecture of a modern transient slope fan (Villafranca fan, Gioia basin–Southeastern Tyrrhenian Sea). *Sed Geol.*, **236**, 211-225.

Ganti, V., Lamb, M.P. and **McElroy, B.** (2014). Quantitative bounds on morphodynamics and implications for reading the sedimentary record. *Nature Comm.*, **5**, Article number: 3298

Garcia, M.H. (2008) Sedimentation engineering; processes, measurements, modeling, and practice. *ASCE Manuals and reports on engineering practice*, **110**.

Gervais, A., Savoye, B., Mulder, T. and **Gonthier, E.** (2006). Sandy modern turbidite lobes: A new insight from high resolution seismic data. *Mar. Petrol. Geol.*, **23**, 485-502.

Gladstone, C., Phillips, J.C. and **Sparks, R.S.** (1998). Experiments on bidisperse, constant-volume gravity currents: propagation and sediment deposition. *Sedimentology*, **45**, 833-843.

Gray, T.E., Alexander, J. and **Leeder, M.R.** (2005). Quantifying velocity and turbulence structure in depositing sustained turbidity currents across breaks in slope. *Sedimentology*, **52**, 467-488.

Grundvåg, S.A., Johannessen, E.P., Helland-Hansen, W. and **Plink-Björklund, P.** (2014). Depositional architecture and evolution of progradationally stacked lobe complexes in the Eocene Central Basin of Spitsbergen. *Sedimentology*, **61**, 535-569.

Hamilton, P., Gaillot, G., Strom, K., Fedele, J. and **Hoyal., D.** (2017). Linking hydraulic properties in supercritical submarine distributary channels to depositional-lobe geometry. *J. Sed. Res*., **87**, 935-950.

Hodgson, D.M., Flint, S.S., Hodgetts, D., Drinkwater, N.J., Johannessen, E.P. and **Luthi, S.** (2006). Stratigraphic evolution of fine-grained submarine fan systems, Tanqua depocentre, Karoo Basin, South Africa. *J. Sed. Res*., **76**, 20– 40.

Hodgson, D.M., Kane, I.A., Flint, S.S., Brunt, R.L. and **Ortiz-Karpf, A**. (2016). Time-transgressive confinement on the slope and the progradation of basin-floor fans: Implications for the sequence stratigraphy of deep-water deposits. *J. Sed. Res*., **86**, 73-86.

Jegou, I., Savoye, B., Pirmez, C. and **Droz, L.** (2008). Channel-mouth lobe complex of the recent Amazon fan: The missing piece. *Mar. Geol*., **252**, 62–77.

Johnson, S.D., Flint, S.S., Hinds, D. and **Wickens, H.d.V.** (2001). Anatomy of basin floor to slope turbidite systems, Tanqua Karoo, South Africa: sedimentology, sequence stratigraphy and implications for subsurface prediction. *Sedimentology*, **48**, 987–1023.

Kane, I.A., Pontén, A.S.M., Vangdal, B., Eggenhuisen, J.T., Hodgson, D.M. and **Spychala, Y.T.** (2017). The stratigraphic record and processes of turbidity current transformation across deep-marine lobes. *Sedimentology*, **64**, 1236–1273

Kneller, B.C. and **Branney, M.J.** (1995). Sustained high-density turbidity currents and the deposition of thick massive sands. *Sedimentology*, **42**, 607-616.

Kneller, B. and **Buckee, C.** (2000). The structure and fluid mechnics of turbidity currents: some recent studies and their geological implications. *Sedimentology*, **47**, 62-94.

Kneller, B. (2003). The influence of flow parameters on turbidite slope channel architecture. *Mar. Petrol. Geol*., **20**, 901-910.

Khripounoff, A., Vangriesheim, A., Babonneau, N., Crassous, P., Dennielou, B. and **Savoye, B.** (2003). Direct observation of intense turbidity current activity in the Zaire submarine valley at 4000 m water depth. *Mar. Geol*., **194**, 151–158. 2003

Lamb, M.P., McElroy, B., Kopriva, B., Shaw, J. and **Mohrig, D.** (2010). Linking river-flood dynamics to hyperpycnal-plume deposits: Experiments, theory, and geological implications. *Geol. Soc. Am. Bull*., **122**, 1389-1400.

Laval, A., Cremer, M., Beghin, P. and **Ravenne, C.** (1988). Density surges: two-dimensional experiment. *Sedimentology,* **35**, 73-84.

Liu, J.T., Wang, Y.-H., Yang, R.T., Hsu, R.T., Kao, S.-J., Lin, H.-L. and **Kuo, F.H.** (2012). Cyclone induced hyperpycnal turbidity currents in a submarine canyon. *J. Geophys. Res*., **117**, C04033.

Lowe, D.R. (1982). Sediment gravity flows: II. Depositional models with special reference to the deposits of high-density turbidity currents. *J. Sed. Petrol*., **52**, 279-297.

Luthi, S. (1981). Experiments on non-channelized turbidity currents and their deposits. *Mar. Geol*., **40**, M59-M68.

Marini, M., Salvatore, M., Ravnås, R. and **Moscatelli, M.** (2015). A comparative study of confined vs. semi-confined turbidite lobes from the Lower Messinian Laga Basin (Central Apennines, Italy): Implications for assessment of reservoir architecture. *Mar. Petrol. Geol*., **63**, 142-165.

McArthur, A.D., Gamberi, F., Kneller, B.C., Wakefield, M.I., Souza, P.A. and **Kuchle, J.** (2017). Palynofacies classification of submarine fan depositional environments: Outcrop examples from the Marnoso-Arenacea Formation, Italy. *Mar. Petrol. Geol.*, **88**, 181-199.

Middleton, G.V. and **Hampton, M.A.** (1973). Part I. Sediment gravity flows: Mechanics of flow and deposition. Pacific Section SEPM, 1-38.

Morris, E.A., Hodgson, D.M., Flint, S.S., Brunt, R.L., Butterworth, P.L. and **Verhaeghe, J.** (2014). Sedimentology, stratigraphic architecture and depositional context of submarine frontal lobe complexes. *J. Sed. Res*., **84**, 763-780.

Mulder, T. and **Alexander, J.** (2001). Abrupt change in slope causes variation in the deposit thickness of concentrated particle-driven density currents. *Mar. Geol*., **175**, 221-235.

Mulder, T. and **Etienne, S.** (2010). Lobes in deep-sea turbidite systems: State of the art. *Sed. Geol*., **229**, 75-80.

Mutti, E. (1977). Distinctive thin-bedded turbidite facies and related depositional environments in the Eocene Hecho Group (South-central Pyrenees, Spain). *Sedimentology*, **24**, 107-131.

Mutti, E. (1992). Turbidite Sandstones, Agip -Instituto di Geologia, Università di Parma, Italy, 275p.

Mutti, E. and **Normark, W.R.** (1987). Comparing examples of modern and ancient turbidite systems: Problems and concepts. In: Marine Clastic Sedimentology: Concepts and Case Studies (Eds. J.K. Leggett and C.G. Zuffa) Graham & Trotman, London, 1-38.

Nelson, C.H., Twichell, D.C., Schwab, W.C., Lee, H.J. and **Kenyon, N.H.** (1992). Upper Pleistocene turbidite sand beds and chaotic silt beds in the channelized, distal, outer-fan lobes of the Mississippi fan. *Geology*, **20**, 693–696.

Normark, W.R. (1970). Channel piracy on Monterey Deep-Sea Fan. Deep-Sea. Deep-Sea Research and Oceanographic Abstracts 17, 837-846.

Normark, W.R. (1978). Fan valleys, channels, and depositional lobes on modern submarine fans: Characters for recognition of sandy turbidite environments. *AAPG Bull.*, **62**, 912-931.

Ouchi, S., Ethridge, F.G., James, E.W. and **Schumm, S.A.** (1995). Experimental study of subaueous fan development. In: Hartley, A.J., Prosser, D.J. (Eds.), Characterization of Deep Marine Clastic Systems. *Geol. Soc. Spec. Publ*., **4**, 13-29.

Palanques, A., Kenyon, N.H., Aloso, B. and **Limonov, A.** (1995). Erosional and depositional patterns in the Valencia Channel mouth: An example of a modern channel-lobe transition zone. *Mar. Geophys. Res*., **17**, 503-517.

Parsons, J.D., Schweller, W.J., Stelting, C.W., Southard, J.B., Lyons, W.J. and **Grotzinger, J.P.** (2002). A preliminary experimental study of turbidite fan deposits. *J. Sed. Res*., **72**, 619-628.

Pirmez, C., Prather, B.E., Mallarino, G., O'Hayer, W.W., Droxler, A.W. and **Winker, C.D.** (2012). Chronostratigraphy of the Brazos-Trinity depositional system, Western Gulf of Mexico: Implications for deepwater depositional models. In: *Application of the Principles of Seismic Geomorphology to Continental -Slope and Base-of-Slope Systems: Case Studies from Seafloor and Near-Seafloor Analogues* (Eds. B.E. Prather, M.E. Deptuck, D. Mohrig, B. van Hoorn and R.B. Wynn). *SEPM Spec. Publ.*, **99**, 112- 143.

Porten, K.W., Kane, I.A., Warchoł, M.J. and **Southern, S.J.** (2017). A sedimentological process-based approach to depositional reservoir quality of deep-marine sandstones: an example from the Springar Formation, north-western Vøring Basin, Norwegian Sea. *J. Sed. Res*., **86**, 1269-1286.

Posamentier, H.W. and **Kolla, V.** (2003). Seismic geomorphology and stratigaphy of depositional elements in deep-water settings. *J. Sed. Res.*, **73**, 367-388.

Pohl, F., Eggenhuisen, J.,Cartigny, M.,Tilston, M., de Leeuw, J. and **Hermidas, N. (2019a).** The Influence of a Slope Break on Turbidite Deposits: An Experimental Investigation. *EarthArXiv*. June 24. doi:10.31223/osf.io/v58gm

Prather, B.E., Booth, J.R., Steffens, G.S. and **Craig, P.A.** (1998). Classification, lithologic calibration, and stratigraphic succession of seismic facies of intraslope basins, Deep-Water Gulf of Mexico. *AAPG Bull.,* **82**, 701-728.

Prélat, A., Hodgson, D.M. and Flint, S.S. (2009). Evolution, architecture and hierarchy of distributary deep-water deposits: a high-resolution outcrop investigation from the Permian Karoo Basin, South Africa. *Sedimentology*, **56**, 2132-2154.

Prélat, A., Covault, J.A., Hodgson, D.M., Fildani, A. and **Flint, S. S.** (2010). Intrinsic controls on the range of volumes, morphologies, and dimensions of submarine lobes. *Sed. Geol*., **232**, 66-76.

Prélat, A. and **Hodgson, D.M.** (2013). The full range of turbidite bed thickness patterns in submarine lobes: controls and implications. *J. Geol. Soc. London*, **170**, 1-6.

Pyles, D.R., Straub, K.M. and **Stammer, J.G.** (2013). Spatial variations in the composition of turbidites due to hydrodynamic fractionation. *Geophys. Res. Lett.*, **40**, 3919-3923.

Richardson, J.F. and **Zaki, W.N.** (1954). The sedimentation of a suspension of uniform spheres under conditions of viscous flow. *Chem. Eng. Sci.*, **3**, 65-73.

Romans, B.W., Castelltort, S., Covault, J.A., Fildani, A. and **Walsh, J.P.** (2016). Environmental signal propagation in sedimentary systems across timescales. *Earth-Science Reviews*, **153**, 7-29.

Saller, A.H., Noah, J.T., Prama Ruzuar, A. and **Schneider, R.** (2004). Linked lowstand delta to basin-floor fan deposition, offshore Indonesia: An analog for deep-water reservoir systems. *AAPG Bull.*, **88**, 21-46.

Saller, A., Werner, K., Sugiaman, F., Cebastiant, A., May, R., Glenn, D. and **Barker, C.** (2008). Characteristics of Pleistocene deep-water fan lobes and their application to an upper Miocene reservoir model, offshore East Kalimantan, Indonesia. *AAPG Bull.*, **92**, 919–949.

Satur, N., Hurst, A., Cronin, B.T., Kelling, G. and **Gürbüz, K.** (2000). Sand body geometry in a sand-rich, deep-water clastic system, Miocene Cingöz Formation of southern Turkey. *Mar. Petrol. Geol*., **17**, 239-252.

Sohn, Y.K. (1997). On traction-carpet sedimentation. *J. Sed. Geol*., **67**, 502-509.

Southard, J.B. and **Mackintosh, M.E.** (1981). Experimental test of autosuspension. *Earth Surf. Proc. Land*., **6**, 103-111.

Spychala, Y.T., Hodgson, D.M., Prélat, A., Kane, I.A., Flint, S.S. and **Mountney, N.P.** (2017a). Frontal and Lateral Submarine Lobe Fringes: Comparing Sedimentary Facies, Architecture and Flow Processes. *J. Sed. Res.*, **87**, 75-96.

Spychala, Y.T., Hodgson, D.M., Stevenson, C.J. and **Flint, S.S.** (2017b). Aggradational lobe fringes: The influence of subtle intrabasinal seabed topography on sediment gravity flow processes and lobe stacking patterns. *Sedimentology*, **64**, 582–608.

Steel, E., Buttles, J., Simms, A.R., Mohrig, D., and **Meiburg, E.** (2017). The role of buoyancy reversal in turbidite deposition and submarine fan geometry. *Geology*, **45**, 35-38.

Stevenson, C.J., Jackson, C.A-L., Hodgson, D.M., Hubbard, S.M. and **Eggenhuisen, J.T.** (2015) Sediment bypass in deep-water systems from modern seafloor, outcrop, subsurface and experimental data. *J. Sed. Res*., **85**, 1058-1081.

Stevenson, C.J., Feldens, P., Georgiopoulou, A., Schönke, M., Krastel., S., Piper, D.J.W., Lidhorst, K. and **Mosher, D.** (2018). Reconstructing the sediment concentration of a giant submarine gravity flow. *Nature Comm*., **9**, Article number: 2616.

Straub, K.M. and **Pyles, D. R.** (2012). Quantifying the Hierarchical Organization of Compensation In Submarine Fans Using Surface Statistics. *J. Sed. Res.*, **82**, 889-898.

Talling, P.J., Paill, C.K. and **Piper, D.J.W.** (2013). How are subaqueous sediment density flows triggered, what is their internal structure and how does it evolve? Direct observations from monitoring of active flows. *Earth-Sci. Rev*., **125**, 244-287.

Tilston, M., Arnott, R.W.C., Rennie, C.D. and **Long, B.** (2015). The influence of grain size on the velocity and sediment concentration profiles and depositional record of turbidity currents. *Geology*, **43**, 839-842.

Twichell, D.C., Schwab, W.C., Nelson, C.H., Kenyon, N.H. and **Lee, H.J.** (1992). Characteristics of a sandy depositional lobe on the outer Mississippi fan from DeaMARC IA sidescan sonar images. *Geology*, **20**, 689–692.

van der Werff, W. and **Johnson, S.** (2003). High resolution stratigraphic analysis of a turbidite system, Tanqua Karoo Basin, South Africa: *Mar. Petrol. Geol*., **20**, 45-69.

Wynn, R.B., Weaver, P.E., Masson, D.G. and **Stow, D.A.V.** (2002). Turbidite depositional architecture across three interconnected deep-water basins on the north-west African margin. *Sedimentology*, **49**, 669-695.

Xu, J.P., Sequeiros, O.E. and **Noble, M.A.** (2014). Sediment concentrations, flow conditions, and downstream evolution of two turbidity currents, Monterey Canyon, USA. Deep-Sea Research I 89, 11-34.

FIGURE CAPTIONS

Figure 1: Width vs length values for lobes deposited in the Karoo Basin (Prélat et al., 2009), the Amazon Fan (Jegou et al., 2008), the Golo Fan (Deptuck et al., 2008), the Kutai Basin (Saller et al., 2008), the Giza Field (Morris et al., 2014) and the Al Batha Turbidite System (Bourget et al., 2010) and their length:width aspect ratios.

Figure 2: A) The experimental set-up consists of three areas: 1) slope with a~~dipping at~~ 11° gradient with a pre-formed channel, 2) basin floor with varying ~~dip~~gradient (0-4°), and 3) horizontal plain which is used to install the UVP probes. B) Set-up of UVP probes in relation to the pre-formed channel. Four UVPs probes are located longitudinal to the channel form. Probe numbers are marked in white.

Figure 3: Schematic of an experimental deposit and the measured parameters.

Figure 4: Erosion/deposition maps of Series I (basin floor angle). Blue colours represent deposition, red colours erosion. As the basin floor becomes steeper (A to E) the deposit

becomes more elongated and the depocenter is relocated further basinwards. Erosional patterns in front of the inlet are an experimental artefact.

Figure 5: Topographic profiles showing the longitudinal geometry of the deposits. A: Run 1 shows the highest thickness of 8.8 cm 1m from the break of slope. The deposit thins subsequently as the basin floor angle increases and the point of maximum thickness shifts farther into the basin. Run 6 for example has a thickness of 6.2 cm 2.7 m from the break of slope. B: Runs with varying concentrations produce two types of geometries. The higher concentration runs (Run 5 and 6) have deposits that reach far into the basin and show their maximum thickness at 3.0 and 2.7 m from the break of slope, respectively, whereas lower concentration runs (Run 7 and 8) have wedge-shaped longitudinal geometries with their maximum thickness directly after the break of slope. C: Runs with different discharges produce similar geometries. However, the onlap of the deposit produced by Run 9 (lowest discharge) is significantly upstream of the break of slope (also see Fig. 10), while Run 10 (highest discharge) produces an area of low sedimentation behind the break of slope. The deposit starts thickening 1.0 m into the basin.

Figure 6: Surface area over distance from the break of slope a proxy of volume distribution. A: Distributions for Series I imply that steeper basin-floor angles are more efficient in transporting sediment resulting in a basinward relocation of the depocentre. B: Distributions for Series II show that higher concentration currents will deposit the bulk volume of sediment farther in the basin, while lower concentration currents aggrade deposits in front of the break of slope and taper downstream. C: Distributions

for Series III display that higher discharges will result in more basinward located depocentres, wheres lower discharges will shift the depocentre upstream.

Figure 7: Erosion/deposition maps of Series II ~~by~~ (changing sediment volume concentration). ~~Currents~~ Deposits ~~with~~from currents~~experiments~~ with lower sediment concentration are~~become~~ shorter.

Figure 8: Cross-section view for different distances behind the break of slope. A: Run 6 shows an indent into its convex up shape near the break of slope indicating increased bypass of the current. B: Convex up shaped geometry of Run 7.

Figure 9: Digital elevation models (DEMs) of the deposits created by changing discharge. A: The deposit of Run 9 (lowest discharge) onlaps high onto the slope. B: The deposits of Run 6 (medium discharge) onlaps at the base of slope. C: The deposit of Run 10 (highest discharge) is detached from the slope by an area of low deposition.

Figure 10: Maximum velocity and flow height graphs for Series I (A), Series II (B) and Series III (C).

Figure 11: A: Diagram of lobe hierarchy dependent compensation; B: Planview relationship between lobe elements forming a lobe. Yellow colours mark sand-prone deposits, grey colours silt-prone deposits (modified from Straub et al., 2012).

Figure 12: Measured lobe element length versus calculated advection lobe element length. Generally, calculated lengths are ~~more than 50~~around 75 % accurate~~. in general.~~

This means that advection length can be used as a first order estimation of lobe element length, although length values are consistently under predicted.

Figure 13: Limitations of the advection length scale approach. A: The method is highly dependent on the input of average grain size. All grain sizes below the d50 are omitted from the length estimation. B: In runs with high concentration and high discharge the depocentre is shifted farther basinwards. The calculated length of the deposit of Run 10 does not only underestimate the length dimensions, but would also omit the main depocentre of the depositional body.

Figure 14: Simplified lobe model showing sand-prone, heterolithic and silt-prone dominated environments. The sandy lobe only represents a small part of the full lobe. A: In planview the silt-prone deposits surround the sandy lobe like a halo. B: Longitudinal cross-section shows that siltstone deposits form an extensive thin layer into the basin.

Table 1: Overview of the experimental parameters for the ten conducted runs.

Table 2: Summary of maximum dimensions and aspect-ratios for the deposits of all conducted runs.

Table 3: Values used to calculate lobe element length. Flow velocity (u, in m/s), flow height (h, in m), settling height (h, in m), settling velocity (w_s, in m/s), and advection length (l_a, in m) .

Table 43: Reconstructed turbidity current velocities from include the Amazon Fan (Jegou et al., 2008), Fan 3, Tanqua depocentre, Karoo Basin (Prélat et al., 2009, Kane et al., 2017), the Golo Fan offshore Corsica (Deptuck et al., 2008, Hamilton et al., 2017) and the Pleistocene Fan, Kutai Basin, Indonesia (Saller et al., 2004, 2008)

The influence of basin setting and turbidity current properties on the dimensions of submarine lobe elements.

Spychala, Y.T.[1]*, Eggenhuisen, J.T.[1], Tilston, M.[1], Pohl, F.[1]

[1]EuroSEDS, Department of Earth Sciences, Utrecht University, 3584 CB Utrecht, NL

*Corresponding author: yts@gmx.de

ABSTRACT

Submarine lobes have been identified within various deep-water settings, including the basin-floor, the base of slope and the continental slope. Their dimensions and geometries are postulated to be controlled by the topographic configuration of the seabed, sediment supply system and slope gradient.

Ten experiments were conducted in a 3D-flume to study the depositional characteristics of submarine lobes associated with 1) different basin floor gradients (0-4°), 2) different sediment concentration of the parent turbidity current (11-19 % Vol), and 3) varying discharge (25 - 40 m^3/h). Most runs produced lobate deposits that onlapped onto the lower slope. Deposit length was proportional to basin-floor angle and sediment volume concentration. A higher amount of bypass is observed in the proximal area as the basin-floor angles get steeper and sediment concentrations higher. Deposits of runs with lower discharge could be traced higher upslope while runs with higher discharge produced an area of low deposition behind the channel mouth, i.e. discharge controlled whether lobe deposits were attached or detached from their channel-levee systems. A particle-advection-length scale analysis suggests that this approach can be used as a first order estimation of lobe element length. However, the estimations strongly depend on the

average grain size used for calculations (e.g. silt is still actively transported after all sand has been deposited) and the method cannot be used to locate the main depocentre. Furthermore, attempted reconstructions of turbidity current velocities from natural systems suggest that the method is not appropriate for use in inversions from more complex composite bodies such as lobes.

Keywords: morphology, turbidity current, experimental study. dimensions, advection length, sand bias

INTRODUCTION

Submarine lobes are high aspect-ratio, sand-rich deposits fed by sediment gravity flows via channels. They are a major component of submarine fans, the largest depositional bodies on the planet, and therefore represent an important archive of palaeo-environmental change (e.g. Prélat et al., 2009; Flint et al.,2011; Romans et al., 2016). Submarine lobe deposits are also of economic interest because of their potential as hydrocarbon reservoirs. Thus, lobe characteristics such as dimensions, geometries, volumes and depositional sand quality are of high interest (e.g. Mulder and Alexander, 2001; Portén et al., 2016).

Traditionally, submarine lobe deposits were described as simple radial bodies that thin and become progressively finer-grained away from an apex (e.g. Normark, 1970; Mutti, 1977; Normark, 1978; Luthi, 1981; Lowe, 1982; Bouma, 2000). However, it has recently been recognized that the geometry of lobe deposits is more complicated (e.g. Nelson et al., 1992; Twichell et al., 1992; Gervais, 2006; Hodgson et al., 2006; Deptuck et al., 2008; Prélat et al., 2009; Etienne et al., 2012; Burgreen & Graham, 2014,

Grundvåg et al., 2014, Spychala et al., 2017a). It has also been observed that lobe dimensions and aspect-ratios do vary significantly within individual submarine fans (Deptuck et al., 2008; Jegou et al., 2008; Saller et al., 2008; Prélat et al., 2009; Bourget et al., 2010; Morris et al, 2014; see Fig. 1). The cause of this variation in lobe dimensions is the focus of this paper. Prélat et al. (2010) proposed that, while lobe volumes have a narrow range, which is independent of the size of the overall deepwater system they are deposited in, lobe geometries and dimensions show strong influence from the local topography and the up-dip supply system. Confinement is seen as a main controlling factor in some publications, dividing systems in unconfined and confined lobes (Prélat et al., 2010), whereas Hamilton et al. (2017) spectulate that supercritical vs. subcritical behaviour connected to slope angles is the main control on lobe dimensions.

Outcrops and seismic datasets allow the in-depth study of lobe facies, internal architecture and plan-view geometries. However, they do not allow for the direct study of the influence of controlling parameters of flow discharge, sand:mud ratio and basin set-up that led to the deposits (Posamentier and Kolla, 2003; Prélat et al. 2010). Laboratory experiments allow the manipulation of specific boundary conditions, and therefore their influence on the deposits can be directly quantified. In addition, instrumental documentation of changes to the flow can be conducted systematically (e.g. Baas et al., 2004; Hamilton et al., 2017). While flume experiments traditionally focus on the behaviour of the flow itself, increasing effort has been invested to also model the development of prominent morphologies of submarine fans (e.g. Luthi, 1981; Ouchi et al., 1995; Parsons et al., 2002; Baas et al., 2004; Pyles et al., 2013; Fernandez et al., 2014; Hamilton et al., 2017, Steel et al., 2017, de Leeuw et al., 2018). Break in slope, channel dimensions, channel hydraulics, interstitial fluid density and grain-size

distribution of the parent flow have been suggested to have an important influence on the architecture of lobes (Baas et al., 2004; Prélat et al., 2010, Cantelli et al., 2011, Fernandez et al., 2014; Hamilton et al., 2017, Steel et al., 2017, De Leeuw et al., 2018). Choi and Garcia (2001) have pointed out that longitudinal and lateral spreading of unconfined flows cannot be looked at in separation. i.e. the amount of lateral spreading governs how far a flow can spread longitudinally.

It is generally assumed that length of turbidity current deposits is primarily determined by the velocity of the flow, settling velocity of the particles and flow thickness (e.g. Mulder and Alexander, 2001; Lamb et al., 2010; Ganti et al., 2014). Ganti et al. (2014) suggested a simple mathematical approximation to determine the advection length (l_a) of a variety of sedimentary features, including submarine fans built up by turbidity currents. Advection length is defined as the horizontal length over which a characteristic particle is transported in the flow before it settles to the ground. This approach deals with three simple parameters: flow velocity (u), average settling height (h_s) and settling velocity of the characteristic particle size (w_s). Whether this advection length method can be used as a first order estimation tool for deposit geometry from turbidity currents is untested, while there are a number of issues that deserve scrutiny. For instance, if the basin slope is not fully horizontal but dipping at a gradient towards the basin, the gravitational pull must be expected to result in turbulence that maintains suspension of the sediment beyond the advection length scale. We find previous considerations of the role of turbulence in advection length estimates to be too simplistic, and this will be discussed in detail later in this paper. Another process that could impact the length of transport on lobes is the concentration-dependence of the settling velocity, for instance through hindered settling (Richardson and Zaki, 1954). Furthermore, the use of different grain sizes for calculationscan lead to very different

estimated length scales, especially in mixed systems that are built by flows that comprise sand and silt grains. An interesting question to investigate is how a single advection length scale based on one characteristic grains size corelates to the areal distribution of facies associations in such mixed systems. Silt-grained sediment is dominantly deposited in lobe fringe and distal lobe fringe environments in natural systems (Prélat et al., 2009; Etienne et al., 2012; Grundvåg et al., 2014; Marini et al., 2015; Spychala et al., 2017a,b) and was suggested to form a wide halo around the sandy lobe proportion as silt will still be transported basinwards and deposits long after the sand-sized grains have settled out. Nonetheless, deep-water studies primarily focus on the sand-prone deposits of submarine fans, creating a sand-prone bias and uncertainties about the real dimensions of deep-water lobes (Boulesteix et al., 2019).

Here, we systematically investigate the influence of basin morphology, volume concentration and discharge of the parent flow on lobe dimensions and geometries, while we keep grain-size distribution and channel morphology constant. Specific aims for the presented study are 1) to study the range of dimensions and geometries observed from changing boundary conditions; 2) to investigate if observed depositional patterns can be related to flow properties; 3) to discuss which factors are controlling the differences in observed deposit shapes; 4) to debate if it is possible to predict dimensions and geometries from velocity (u) and settling velocity (w_s) alone, and, if yes, what are the caveats of this method? and, 5) to compare the discrepancy of predicted advection length using sand or silt particles as a characteristic parameter and discuss the role of silt-prone sediments as part of lobe deposits.

METHODS

Set-up and procedure

The experiments are conducted in the Eurotank Flume Laboratory at Utrecht University. The Eurotank is 6 m wide and 11 m long. The tank was filled up with water to a level of 1.2 m (Fig. 2A). The bathymetry created in the tank consisted of a 11° slope, a variable gradient (0-4°) basin floor, and a horizontal termination at the end of the set-up that was used for setting up the measurement equipment (Fig. 2A). A channel (0.8 m wide and 0.05 m deep) with levees was built on the slope and restored to the same dimensions after each run. The channel dimensions are chosen to conform with the Run 4 presented in de Leeuw et al. (2018) They found that these channel dimensions resulted in only minor modification of the channel shape by erosion or deposition. This is desirable here because the focus of this paper is on lobe characteristics and channel evolution is ideally kept to a minimum. . The entire set-up is covered by unconsolidated substrate with a similar composition to that used to generate the turbidity currents (sand/ silt mixture with d50 of 133 μm) allowing for erosion by the incoming turbidity currents. Shields scaling (de Leeuw et al., 2016, Pohl et al., 2019) was applied to create turbidity currents that allow for investigation of depositional processes.

The experimental series consist of ten runs in total; Runs 1-4 and 6 investigate the influence of the basin-floor gradient (Series I), Runs 5-8 focus on the influence volume concentration of the sediment (Series II) and Runs 6,9 and 10 on different discharge (Series III). The values for each parameter in the individual runs are shown in Table 1. A mixture of sand and water (total volume: 0.9 m^3) with varying sediment volume concentrations (Series II) was prepared in a separate mixing tank. Sediment used is a mixture of 75% quartz grains (density: 2650 kg/m^3) and 25% ground glass (2500 kg/m^3)

and has a median grain size (d50) of 133 μm. The mixture is pumped into the Eurotank using a radial flow pump. The discharge rate was set to 30 m^3/h for most of the runs except for the discharge series Run 9 and 10 (Table 1). The discharge was monitored with a discharge meter (Krohne Optiflux 2300). Experiments were run until the mixing tank was drained. Depending on the discharge this took between 80 and 100 seconds. The mixture then entered the experimental set-up through an inlet box which has a 1 m section of non-erodible material attached to its front and gradually expanding side-walls. A small scour is generated where the flow passes onto the erodible section of the slope. As this erosion is an experimental artifact, it will be neglected in the evaluation of depositional and erosional patterns.

Data acquisition and processing

UVP

Velocity profiles of the turbidity currents were collected in four different locations (Fig.2B) using Ultrasonic Velocity Profiler probes (UVPs). The probes were set up 18 cm above the bed to prevent obstruction of the flow. They were oriented in a 60° angle to the local preformed bed. Bed-parallel velocity is calculated through trigonometry with the assumption that there is no average bed-perpendicular velocity and that the mean flow direction is in the vertical plane of the angled UVP beam. As the bed is the datum for the UVP data, and its position varies throughout the run due to erosion and deposition, the first step of the data processing phase involves identifying the temporal changes in bed position. Velocity profiles and flow thickness were averaged for individual runs for the body of the current. Velocity profiles and flow thicknesses for individual runs were averaged for the body of the flow by omitting the first 5 second (current head) and last 10 seconds (current tail) from the dataset

176

177 *DEM*

178 Before and after each experiment a laser scan of the topography within the tank is
179 conducted. These are used to create digital elevation models (DEMs) with a horizontal
180 resolution of 2x2 mm and maps of the deposition and erosion that occurred during the
181 runs. Changes in elevation less than 5 mm were omitted in the erosion/deposition maps
182 to avoid interference of bed reworking (migration ripples) with depositional trends.
183 After each experiment the dimensions (width, length, and thickness) of the lobe body
184 and its relation to the base of slope (detached or attached) were documented (Fig. 3), as
185 well as the channel length and its gradient. Width and length were measured with a tape
186 measure in the tank and confirmed in the DEMs, whereas thickness was established by
187 looking at the longitudinal cross-sections created from the DEMs. Deposit lengths is
188 defined as the length from the onset of deposition of the lobate deposit to its terminus.
189 Strike-cross-sectional areas, which are a proxy for the depocentre, were determined by
190 subtracting the DEMs of the initial topography from those of the post experimental
191 topography.
192 Deposits are interpreted as attached if their onset of deposition is on the slope, whereas
193 deposits that show distinctive thickening on the basin floor are interpreted as detached.

194

195 **RESULTS**

196 **Morphology of lobe deposits**

197

198 In this section, we present the dimensions and geometries of the deposits in detail in
199 association with the series they have been conducted in. A summary of the dimensions
200 can be found in Table 2. Aside from the below described characteristic all of the

experimental deposits exhibit a ripple-field to the margins of the main sand body that is best developed to the frontal margin of the deposit.

Series I: basin-floor slope

Runs 1-4 and 6 (Series I) study the influence of the gradient of the basin floor on deposit dimensions and morphology. As the basin-floor angle increases from 0° to 4°, the length of the deposit increases from 310 cm to 383 cm, whereas the width of the deposit decreases from 186 cm to 139 cm (Table 2 and Fig.4). This means that aspect ratios (L/W) vary from 1.7 to 3.2 (Table 2). While the maximum thickness only shows slight variations from 8.8 to 6.2 cm, the location of the thickest part of the deposit is situated distinctly farther from the break-of-slope as the basin-floor becomes steeper (Fig. 5). As the point of maximum thickness is located further downstream, more of the sediment volume also becomes progressively accumulated farther downstream, in effect relocating the depocentre out onto the basin floor (Fig. 6A). All deposits have prominent lobate cross-sections. The exception is Run 6 which shows a small indent (1 cm) to the generally convex top of the deposit in the proximal area , for the first 50 cm after the break-of-slope (Fig. 8A). All deposits, except the one formed by Run 1, onlap onto the slope (Fig. 5).

Series II: sediment volume concentration

Runs 5-8 (Series II) investigate the effect of varying sediment concentration. Results indicate that deposit length is proportional to concentration (Figs. 5C and 8), i.e. the run with the highest sediment concentration (Run 5; 19% Vol) is the longest (465 cm), whereas the run with the lowest concentration (Run 8; 13% Vol) is the shortest (340

cm). Deposits of Run 6 (17% Vol) and Run 7 (15% Vol) are 444 cm and 390 cm long, respectively (Fig. 9). Width dimensions do not show much variability (Table 2) ranging from 143 cm to 139 cm. It is worth noting that Run 8, which has the lowest sediment concentration, has a narrower width of 123 cm. Aspect ratios (L/W) range from 2.7 to 3.4 (Table 2) which means that these deposits are highly elongated. Maximum thickness values show a clear decrease with lower sediment concentrations of the flow (Fig. 5). While a flow with 19% Vol has a deposit with the maximum thickness of 7.8 cm, a flow of 13% Vol has a deposit with a maximum thickness of 5.6 cm. In Series II, two distributions of sediment volume can be observed (Fig. 6B). The runs with the higher concentration (Run 5 and 6) have most of their sediment volume deposited in the intermediate to distal part of the deposit while the runs with lower sediment concentration (Run 7 and 8) have most of their volume deposited in the proximal area. Cross-sections show small indents to the convex tops of the deposit for Run 5 and 6 (between 0.5 and 1 cm; up to 1.5 m from the break-of-slope), while Run 7 and 8 show prominent convex lobe geometries throughout the deposit (Fig. 8B). All runs of Series II onlap onto the slope. Deposition in the channel becomes more prominent with decreasing sediment concentration of the flow.

Series III: Discharge

Runs 6, 9 and 10 (Series III) were conducted to examine the consequence of changing discharge to the dimensions of the resulting deposits. There is no observable trend in the length of the deposits associated with higher or lower discharge, in fact a discharge of $30 m^3/h$ (Run 6) produces a slightly longer deposit (444 cm) than a discharge of $40 m^3/h$ (Run 10; 430 m). The same is true for the width of the deposits (Table 2), that vary between 143 and 118 cm, and maximum thickness that range from 5.6 to 6.9 cm

(Fig. 5), but show no correlation to discharge changes. Aspect ratios (L/W) range from 3.1 to 3.4 (Table 2). The main depocentres for the resulting deposits are located in an intermediate to distal position, with the exception of Run 9 (lowest discharge; 25m^3/h) that has more longitudinal uniformity in its depositional thickness (Fig. 6C). The main difference between the three runs is the point of onset of deposition (Fig. 9). This point is located further down-dip with higher discharges. While the deposit of Run 9 onlaps high up on the slope (after 190 cm of slope length) shortening the total slope length, the deposit of Run 6 onlaps at 210 cm at the base of the slope, and the deposit of Run 10 is detached from the slope (250 cm from the inlet). An area of low deposition is located between the break-of-slope and the deposit for Run 10 (Fig. 9). The deposit shows irregular geometries for 2 m after the break of slope before the deposit thickens and develops a convex geometry in cross-section. Deposits of Run 9 fill the channel form upslope, while deposition from Run 6 and 10 drape the channel form while keeping it with the same dimensions although slightly shallower (4.5 cm instead of 5 cm depth).

Flow properties

Flow velocities

At the break of slope the average velocity for the runs of Series I (Runs 1,2,3,4 and 6) varies from 0.64 m/s to 0.53 m/s with no observable trends in association with change in the downstream basin floor angle (Fig.10A). However, at the position of UVP 7 (Fig. 2B) a pattern starts to develop: Run 6 which corresponds with the steepest basin floor (4°) maintains velocities of 0.34 m/s, whereas the maximum velocity decreases more abruptly with shallower basin-floor gradients and most with a horizontal basin floor (0.2 m/s).

For runs with changing concentration (Series II; Fig. 10B) it can be stated that runs with higher sediment volume concentration (Run 5 and 6) show slightly higher channel exit velocities (0.62 m/s and 0.63 m/s) than those with lower sediment volume concentrations (Run 7: 0.61 m/s; Run 8: 0.54 m/s). The trend becomes more prominent downstream, and velocities correlate positively with sediment concentration at the locations of UVP probes 6 and7. A similar trend can be observed in Series III (Fig. 10C), where runs with higher discharge have higher initial maximum velocities at the break of slope where the flow experiences the loss of confinement and a lower velocity decay rate.

Flow thickness

Flow thickness doesn't show any clear trends for Series I and III (Fig. 10). In Series II it could be observed that runs with lower sediment volume concentrations (Run 7 and 8) have lower initial flow thicknesses and may thicken downstream (Run 8), while runs with higher sediment volume concentration (Run 5 and 6) are thicker on the break of slope and gradually thinner downstream.

DISCUSSION

Controlling factors of lobe length and geometries

The runs of Series I suggest that deposits get subsequently longer, narrower and thinner when the basin-floor angle is increased. This is due to slower loss of streamwise velocity as gravity forces acting on the current counteract its deceleration through loss of excessive density as the flow deposits sediment. There is a lag time until the current adjusts to the new conditions on the basin floor (Mulder and Alexander, 2001) therefore

300 the correlation in flow deceleration with basin-floor angle can best be observed in UVP
301 7 (Fig. 10A). The deposit of Run 1 detached from the slope as sediment suspension is
302 enhanced as energy from downslope travel needs to be dissipated at this abrupt break
303 in slope (11°; e.g. Mulder and Alexander, 2001; Gray et al., 2005), Following this
304 enhanced suspension, grains depositaccording to flow velocity and settling velocity, i.e.
305 the faster the flow the further detached the lobe deposit . Successively the current loses
306 its capacity to carry the bulk of its sediment on the horizontal basin floor, and becomes
307 strongly depletive (Cantero et al., 2014; Eggenhuisen et al., 2017). In contrast to this
308 scenario, basin floor angles that are more inclined enable sediment to be bypassed more
309 efficiently through the basin, eventually relocating the depocentre of the lobe element
310 (Run 6; Fig. 6A).
311 The outcome of Series II indicates that changing volume concentration primarily
312 controls deposit length and the position of the depocentre, while deposit width does not
313 seem to be much influenced. This conforms with observations made on enhanced
314 transport efficiency associated with higher initial densities (Laval et al., 1988;
315 Gladstone et al., 1998; Al Ja'Aidi et al., 2004). The extension of deposition further into
316 the basin can be explained with two mechanisms. Firstly, higher concentration runs
317 have higher initial velocities at the break of slope compared to low concentration runs
318 due to more excess density (Run 8 vs. Run 5; Fig. 10B), i.e. their driving force is larger.
319 Additionally, higher concentration runs exhibit less velocity-loss as they travel over the
320 basin floor, because the overall sediment concentration of the current throughout
321 remains higher compared to low concentration runs. The elongated geometry of the
322 deposit and volume distribution of higher concentration flows suggest that the sediment
323 concentration has reached a limit where hindered settling (Richardson and Zaki, 1954)
324 has at least a partial influence (Kneller and Branney, 1995). Hindered settling refers to

the decrease in settling velocity of particles due to the interaction with other particles in the fluid. Decreased settling velocities cause the sediment to be advected farther into the basin before it settles.Also, indents in the convex tops of the lobate deposits (Run 5 and Run 6; Fig. 8A) point to an increased bypass rate in the proximal axial area of the deposits which explains the relocation of the depocenter farther downstream. These indent morphologies may be (a precursor of) distributary lobe-top channels (see Jegou et al., 2008). It remains to be tested if they represent long-term conduits (Mutti and Normark, 1987) or if they will be filled in by the next incoming event.

Series III suggests that changing discharge does not affect the length of the deposits significantly, but steers whether the deposits are attached or detached from the slope. As higher discharge runs have higher velocities (Fig. 10) they have a higher capacity to transport sediment past the break of slope. Run 10 with the highest discharge transports the sediment farthest out into the basin producing the most elongated lobe element deposit (L/W: 3.4).

In summary, sediment suspension is maintained farther into the basin by steeper basin-floor slope, higher flow discharge, and higher sediment concentrations. The effect on the dimensions of the deposit differ, though: increased slope changes the planform dimensions, increased sediment volume concentration moves the depocenter farther into the basin, and increased discharge controls the point of onset of deposition , while leaving the deposit dimensions more or less the same.

Level of hierarchy

When comparing experimental data to field data the proper level of hierarchy has to be established (cf. Hamilton et al., 2017) to make useful statements. We recognise that a lobe is a composite body comprised of predominantly compensational stacked lobe

elements, that are themselves built of several beds (Deptuck et al., 2008; Prélat et al., 2009; Mulder & Etienne, 2010; Prélat et al., 2010; Bernhard et al., 2012; Etienne et al., 2012; Grundvåg et al., 2014; Marini et al., 2015; Picot et al., 2016; Zhang et al., 2016; Spychala et al., 2017a,b; see Fig. 11). This complexity cannot be modelled by single flow-event experiments. However, it is documented that strength of compensation decreases with lower hierarchical levels (Straub and Pyles,2012), as bed-scale stacking is laterally constrained by the genetically related channel resulting in more or less aggradationally stacked beds that form lobe elements (Fig. 11). This means that small hierarchical units like lobe elements form by weakly compensational stacked beds and their dimensions will ultimately be similar to those of their building blocks (beds). The fact that it is possible to interpret lobe elements in the field through the facies similarity of the beds that form them (e.g. Prélat et al., 2009; Prélat and Hodgson, 2013) further strengthens the assumption that the depositional area has stayed relatively stable during their sedimentation. Therefore, we suggest that observations made in single experimental flows can also be used to compare against lobe element geometries.

Lobe dimensions in natural systems

Prélat et al. (2010) suggested that confinement is the main force behind the division of thick and areally small, and thin, but areally extensive, lobe deposits. This was already debated by Hamilton et al. (2017), who stated that higher slope angles can produce thicker lobes relative to their area without the need of confinement. Our experiments confirm this finding somewhat for lobe elements, although we show that the basin-floor angle does play as important a role as the slope angle. This suggests that lobe element deposited in relatively steep intraslope basins (e.g. Prather et al., 1998; Adeogba et al., 2005; Gamberi and Rovere, 2011; Barton et al., 2012; Pirmez et al., 2012) have

different geometries from lobe elements deposited on nearly horizontal basin floors. However, lobes are composite bodies formed by several lobe elements creating significantly larger deposits. It is to be expected that confinement has an influence on lobe element stacking patterns (aggradational vs. compensational stacking), which will determine if the lobe body itself is thick and areally small, or thin and areally wide. Therefore, confinement cannot be dismissed as an important factor on the composite lobe bodies.

Increased sediment supply (sediment volume concentration and/or sediment discharge) to the basin, whether as a response to relative sea-level fall and/or progressive confinement and increase of turbidity current efficiency (Mutti, 1992; Gardner et al., 2003; Kneller, 2003; Hodgson et al., 2016), is thought to steer progradation of the turbidite system into the basin. Our experiments conform to this model: runs with the highest sediment volume concentration and highest discharge (Run 5 and Run 10) are able to bypass more sediment basinwards. Increased bypass is marked either by an indent in the lobe element top or an area of relative low sedimentation rate that effectively detaches the lobe element deposit from the slope. In contrast, runs with low sediment concentration and discharge (Runs 8 and 9) may represent lobe elements formed during waning sediment supply to the basin through raising relative sea-level and/or channel system aggradation and widening.

This suggests that lobe deposits formed during low vs. high sediment supply may have distinctive morphologies as well as relations with the channelized slope, raising the question if the erosive channel-lobe transition zone (e.g. Palanques et al., 1995; Wynn et al, 2002; Hofstra et al., 2015, Pohl et al., 2019) is a transient feature and therefore rarely observed in ancient outcrops (cf. Brooks et al., 2018).

Can we estimate lobe element dimensions with simple mathematical assumptions?

Advection length, which is defined as the horizontal length of over which a characteristic particle is transported in the flow before it is deposited, has been proposed as a simple method to establish length scales of turbidity current deposits (Mulder and Alexander, 2001; Lamb et al., 2010; Ganti et al., 2014). It deals with three parameters only: flow velocity (u, in m/s), settling height (h, in m) and settling velocity (w_s, in m/s). Advection length of a sediment particle (l_a, in m) is defined as:

$$l_a = uh_s/w_s \quad (1)$$

We compare measured results from our experimental runs with calculated advection length values to test if the advection length approach leads to accurate first order estimations on lobe element length scales. To this end we use the average velocities reported from UVP 4 at the break of slope where the currents enter the unconfined basin floor and start spreading and depositing. Ganti et al. (2014) propose to use an average settling elevation as the characteristic vertical scale. This takes into account the density stratification of turbidity currents (Kneller and Branney, 1995; Sohn, 1997; Amy et al., 2005, Cartigny et al., 2013; Cantero et al., 2014; Tilston et al., 2015), which causes the majority of sediment to be suspended low in the flow. However, in our analysis we are initially interested in predicting the length scale of the lobe elements, which is set by settling of advected particles that were initially at the top of the flow. We therefore choose the flow thickness as the relevant vertical length scale. Finally, we used the d_{50} of the initial suspension (d_{50}= 133µm) as the characteristic grain size. The settling velocity for this grainsize was calculated to be 1.23 cm/s (Ferguson and Church, 2004). All calculated advection lengths and measured deposit lengths as well as used parameters can be found in Table 3.

Generally, calculated lengths are around 75% accurate compared to measured deposit lengths (Table 3; Fig. 12), with the exception of the calculated advection lengths of Run 1, which will be discussed separately below. This means that advection length can be used as a first order estimation of lobe element length, although length values are consistently under predicted (Fig.12). We propose that this under prediction is due to several factors. Firstly, the equation does not account for the effect of turbulence in turbidity currents (Middleton and Hampton, 1973; Southard and Mackintosh, 1981; Kneller and Buckee, 2000; Shringapure et al., 2012) and secondly, the result strongly depends on the chosen grain size and representative settling height used for calculation. Settling is counteracted by turbulent mixing, and grains will therefore remain in suspension longer in the presence of turbulence This effect does not rely on an-isotropy of turbulent statistics (cf. Ganti et al. 2014), but on positive correlation between velocity and concentration fluctuations: upwards moving patches of fluid advect higher sediment concentrations upwards, while downwards moving patches of fluid advect lower sediment concentrations downwards. These correlated fluctuations average out to an upwards positive flux of sediment that works against the settling of sediment (e.g. Garcia, 2008). In a steady flow that bypasses all of its sediment (*sensu* Stevenson et al., 2015), the settling flux is entirely balanced by the turbulent advection flux. In a depletive, but still turbulent turbidity current, the turbulent advection flux partially counteracts settling, and it is thus expected to delay deposition and carry sediment beyond the distances predicted by the advection length. The advection length resulted in the most accurate prediction for Run 1 (102 % accurate; Fig. 12). The turbidity current in Run 1 travelled onto a horizontal basin-floor, and became highly depletive after passing the break of slope. We conclude that the advection length as estimated

449 from the turbidity current structure at the break of slope is a very accurate
450 approximation of lobe element length in situations where the flows are highly depletive
451 and deposition starts on the basin floor. Factors that increase the efficiency of sediment
452 transport into the basin (*sensu* Mutti and Normark, 1987), such as steeper basin floor-
453 angles, and higher sediment concentration and discharge, lead to less accurate
454 underpredictions of lobe element length.
455 A note should be made regarding the use of a constant advection velocity to estimate
456 the advection length scale. Turbidity currents slow down while they flow over lobes
457 and deposit their sediment. The flow velocities were generally decreased to 62-34% at
458 the distal edge of the sandy deposits when compared to the velocity at the location of
459 UVP4. A more complicated advection settling model would account for this decrease
460 in advection velocity, which would result in further under-prediction of lobe element
461 length. This indicates that the efficiency effects described above are likely even more
462 significant than indicated by the appearance of data in Table 3 and Figure 12.
463
464 Length estimations with the advection length approach have to be carried out keeping
465 in mind that the final result is strongly linked to the used "characteristic" grain size and
466 representative height (Fig. 13A). For example, in this case we have used a d_{50} of 133
467 μm (fine sand) biasing our result to the sand grains in our currents. The effect on
468 estimated lobe element dimensions by omitting silt particles is discussed below. In
469 addition, although advection length is useful to predict dimensions for specific grain
470 sizes, it is still important to have a firm understanding of the overall deposit geometry
471 to pinpoint the main depocentre and its relation to the slope (attached vs. detached.) The
472 principles behind advection length (a simple settling from a stratified flow, with lowest
473 and coarsest grains settling fastest) suggests a simple tapering wedge shape for the

created deposit with the main depocentre located proximal to the break of slope. However, basin-floor slope, high concentration, and high discharge shift the depocentre farther basinwards. Figure 13B illustrates how the calculated length of the deposit of Run 10 does not only underestimate the dimensions, but also poorly characterises the depocentre position of the lobe element.

Can we use advection length to reconstruct turbidity current velocities from natural systems?

Advection length is a simple method to estimate first order length scale for the deposits resulting from our experiments. The corollary of successful prediction is that the method can also be used for inversion modelling. The question thus arises whetherwe could also use this method to give us an idea of the velocities of typical turbidity currents that have deposited natural systems. The data chosen to test this encompass four systems whose lobe dimensions, grain sizes and channel depth close to the channel-lobe transition zone were reported. Channel depth values were taken as an estimation for the flow height. Care was taken to ensure lobe dimensions used conform to the same hierarchical level. The datasets chosen include the Amazon Fan (Jegou et al., 2008), Fan 3, Tanqua depocentre, Karoo Basin (Prélat et al., 2009, Kane et al., 2017), the Golo Fan offshore Corsica (Deptuck et al., 2008; Hamilton et al., 2017) and the Pleistocene Fan, Kutai Basin, Indonesia (Saller et al., 2004, 2008). Table 4 shows all calculated velocities for these four systems.

With the exception of the reconstructed velocities from the Pleistocene Fan of the Kutai Basin (1.75 – 9.1 m/s) all the calculated values reconstructed from lobe measurements are deemed far too high (> 10 m/s) to be sensible in respect to other measured (0.4- 3.5 m/s depth-average flow velocity; Khripounoff et al., 2004; Cooper et al., 2012; Liu et

al., 2012; Xu et al., 2014) and estimated (3.8 m/s depth-average flow velocity; Stevenson et al., 2018) turbidity current velocities from natural systems that are not caused by major earthquakes (up to 20 m/s; see Talling et al., 2013). However, using lobe element dimension from Fan 3 of the Karoo Basin instead of lobe dimensions, a much more reasonable value of 4.2 m/s for the current velocity is estimated, although this is still somewhat high (Table 4). Our experiments taught us, that advection length is in average about 75% accurate. With that in mind calculated velocities are likely to be too high even on the lobe element scale.

Still, the fact that calculated velocities for lobe elements seem more reasonable than for lobes underlines anew the composite nature of lobe deposits that is a sum of their lobe element dimensions and stacking patterns which are in turn affected by the properties of incoming turbidity currents, their modification through the channel fairways and underlying topography. A lobe formed by progradational stacked lobe elements would for example result in overestimated flow velocities with this approach due to the successive basinward change of the transition from channel to lobe element as sediment is bypassed through the development of distributive channels that extend farther into the basin). On the other hand, lobe elements that are aggradationally stacked to form a lobe will give more reasonable estimations of current velocities. In addition, the maintenance of suspension into the basin through basin setting and sediment concentration of the turbidity current are other important factors that need to be taken into account as they can cause hindered settling and/or progradation into the basin.

Depositional trends sand vs. silt

523 Lack of exposure, insufficient seismic resolution, and bias towards sand-prone lobe
524 deposits have impeded the estimation of length scales of the silt-prone deposits of the
525 lobe distal fringes to be established, although they can create features of 100 meters
526 thickness when lobe deposition experiences lateral confinement (cf. aggradational lobe
527 fringes, Spychala et al., 2017b;Boulesteix et al., 2019). Our experiments enable us to
528 give first quantitative assumptions on the distance silty material is transported and
529 deposited after all sand has been deposited from the flow.
530 For Run 8 UVP 7 captures the transition from sand-prone deposits to silt-prone deposits.
531 Average velocities at this point are still at 0.24 m /s. Settling velocities of silt sized
532 grains are much smaller that for the sand (0.0014 m/s vs. 0.014 m/s). If we use the
533 simple advection length method we can estimate that silt will be deposited for another
534 9.2 m (see Table 3) in a longitudinal direction, effectively changing lobe element length
535 from 3.4 m to 12.6 m.
536 Consequently, we have to start thinking of lobes in a different way than before. The
537 sand-prone part (lobe axis and off-axis environments) of a lobe only covers a small
538 proximal portion of the whole deposit (Fig. 14) and transitions laterally into heterolithic
539 packages that form the lobe fringes. The dimensions of the lobe fringes are governed
540 by the variations in dimensions and the manner of stacking between beds and lobe
541 elements. Finally, silt-prone distal fringes are the most areally widespread parts of lobes
542 (Fig. 14). This results further strengthens the argument that several metres-thick
543 siltstone intervals named “lobe fringe complexes” or “interlobes” (Prélat and Hodsgon,
544 2013; Spychala et al., 2017a) separating lobe complexes are formed by autogenic
545 processes (Prélat et al., 2009; Spychala et al., 2017a, Boulesteix et al., 2019) instead of
546 genetical unrelated sedimentation (Satur et al., 2000; Johnson et al., 2001; Van der
547 Werff and Johnson, 2003; Hodgson et al., 2006; Mulder and Etienne, 2010; McArthur

548 et al., 2017), and may be traced laterally or up-dip into sand-prone lobe complexes that
549 are located up to several kilometers away. In fact, Boulesteix et al. (2019) show that
550 distal lobe fringes of Fan 3 of the Skoorsteenberg Fm. (Karoo Basin, SA) extended
551 more than 18 km beyond the sand-stone pinchout.
552

553 **CONCLUSIONS**

554 Ten experimental runs were performed to test the influence of basin geometry, sediment
555 volume concentration and discharge on lobe element dimensions and the architecture
556 of their depositional bodies. The experimental lobe element length is proportional to
557 basin-floor angle and sediment volume concentration, whereas discharge is the main
558 factor controlling the onset of lobe element deposition. Higher amounts of bypass
559 behind the break of slope are observed with steeper basin-floor angles, higher
560 concentration and higher discharge. Future research should aim to cover multiple
561 successive runs to test how these initially formed depositional bodies develop over time.
562 Flow properties show only subtle differences.
563 Our results suggest that lobe element deposits formed during different stages of the
564 sediment supply cycle have pertinent different geometries We tested the accuracy of
565 estimating lobe element dimensions with simple advection length calculations. On a
566 first order this method gives a good prediction of the length of lobe element deposits
567 created in our experiments. However, a consistent under prediction of length scales is
568 observed, because maintenance of sediment suspension into the basin through either
569 turbulence production (basin floor slope and flow discharge) is neglected. Attempts to
570 reconstruct turbidity current velocities that have deposited natural systems additionally
571 indicate, that this approach is hierarchy dependent and cannot be expected to yield
572 reasonable results for higher order composite sedimentary bodies, such as lobes and

lobe complexes, that are built by a multitude of turbidity currents over an extended period of time.

Finally, we established that reconstructions of lobe geometries are biased towards their sandy parts, even though silt-prone deposits are still deposited long after all the sand grains have been depleted. This is partly due to missing outcrop exposures, seismic resolution, and partly due to a general bias to sand-prone lobe deposits. This outcome strengthens the interpretation of silt-prone intervals (termed distal lobe fringes or intralobes) to be formed by autogenic process of lobe deposition rather than representing background sedimentation.

ACKNOWLEDGEMENTS

This project was funded by NWO (grant #NWO-ALW-Vidi-864.13.006), ExxonMobil, Shell and Equinor for which we are thankful. Thony van der Gon-Netscher and Han de Witte supplied technical support to the experimental work. Reviews by Sedimentology Associate Editor Kyle Straub and reviewer Elisabeth Steel greatly improved the manuscript.

REFERENCES

Adeogba, A.A., McHargue, T.R. and **Graham, S.A.** (2005). Transient fan architecture and depositional controls from near-surface 3-D seismic data, Niger Delta continental slope. *AAPG Bulletin* **89**, 627-643.

Al Ja'aidi, O.S., McCaffrey, W.D. and **Kneller, B.C.** (2004). Factors influencing the deposit geometry of experimental turbidity currents: implications for sand-body

architecture in confined basins. In: *Confined Turbidite Systems* (Eds S.A. Lomas and P. Joseph). Geological Society, London*, Spec. Publ.*, 222, 45-58.

Amy, L.A., Hogg, A.J., Peakall, J. and **Talling, P.J.** (2005). Abrupt transitions in gravity currents. *J.Geophys. Res.* **110**, F03001.

Baas, J.H., Van Kesteren, W. and **Postma, G.** (2004). Deposits of depletive high-density turbidity currents: a flume analogue of bed geometry, structure and texture. *Sedimentology* **51**, 1053-1088.

Barton, M.D. (2012). Evolution of an Intra-Slope Apron, Offshore Niger Delta Slope: Impact of step geometry on apron architecture. In: *Application of the principles of seismic geomorphology to continental -slope and base-of-slope systems: Case studies from seafloor and near-seafloor analogues* (Eds. B.E. Prather, M.E. Deptuck, D. Mohrig, B. van Hoorn and R.B. Wynn), *SEPM Spec. Publ.,* 99, 181- 197.

Bouma, A.H. (2000). Fine-grained, mud-rich turbidite systems: Model and comparison with coarse-grained, sand-rich systems. In: *Fine-grained Turbidite Systems* (Eds. A.H. Bouma and C.G. Stone) *AAPG Memoir 72/SEPM Spec. Publ.,* 68, 9-19.

Boulesteix, Kévin, Miquel Poyatos-Moré, Stephen Flint, David M. Hodgson, Kevin G. Taylor, and **Gareth R. Parry.** (2019). Sedimentary Facies and Stratigraphic Architecture of Deep-water Mudstones Beyond the Basin-floor Fan Sandstone Pinchout. *EarthArXiv*. July 9. doi:10.31223/osf.io/3qrew

Brooks, H.L., Hodgson, D.M., Brunt, R.L., Peakall, J., Hofstra, M. and **Flint, S.S.** (2018). Deep-water channel-lobe transition zone dynamics: Processes and depositional architecture, an example from the Karoo Basin, South Africa. *Geol. Soc. Am. Bull.,* **130**, 1723-1746.

Burgreen, B. and **Graham, S.** (2014). Evolution of a deep-water lobe system in the Neogene trench-slope setting of the East Coast Basin, New Zealand: Lobe stratigraphy and architecture in a weakly confined basin configuration. *Mar. Petrol. Geol.,* **54**, 1-22.

Bourget, J., Zaragosi, S., Mulder, T., Schneider, J.-L., Garlan, T., Van Toer, A., Mas, V. and **Ellouz-Zimmermann, N.** (2010). Hyperpycnal-fed turbidite lobe architecture and recent sedimentary processes: Acase study from the Al Batha turbidite system, Oman margin. *Sed. Geol.,* **229**, 144-159.

Cantelli, A., Pirmez, C., Johnson, S. and **Parker, G.** (2011). Morphodynamic and Stratigraphic Evolution of Self-Channelized Subaqueous Fans Emplaced by Turbidity Currents. *J. Sed. Res*., **81**, 233-247.

Cantero, M., Balachandar, S., Cantelli, A. and **Parker, G.** (2014). A simplified approach to address turbulence modulation in turbidity currents as a response to slope breaks and loss of lateral confinement. Environment Fluid Mechanics, **14**, 371-385.

Cartigny, M., J.B., Eggenhuisen, J.T., Hansen, E.W.M. and **Postma, G.** (2013). Concentration-Dependent Flow Stratification In Experimental High-Density Turbidity Currents and Their Relevance To Turbidite Facies Models. *J. Sed. Res*., **83**, 1047-1065.

Choi, S.-U. and **Garcia, M.H.** (2003). Spreading of Gravity Plumes on an Incline. *Coastal Engineering Journal*, **43:4**, 221-237,

Cooper, C., Wood, J. and **Andrieux, A.** (2013). Turbidity current measurements in the Congo Canyon, OTC Abstract 23992. Offshore Technology Conference, 6–9 May, Houston, Texas 12 pp.

de Leeuw, J., Eggenhuisen, J.T. and **Cartigny, M.J.B.** (2016). Morphodynamics of submarine channel inception revealed by new experimental approach. *Nature Comm*., **7**, Article number: 10886.

de Leeuw, J., Eggenhuisen, J.T., Spychala., Y.T., Heijnen, M.S., Pohl, F. and **Cartigny, M.J.B**. (2018). Sediment Volume and Grain-Size Partitioning between Submarine Channel-Levee Systems and Lobes: An Experimental Study. *J. Sed. Res*., **88**, 1-18.

Deptuck, M.E., Piper, D.J.W., Savoye, B. and **Gervais, A.** (2008). Dimensions and architecture of late Pleistocene submarine lobes off the northern margin of East Corsica. *Sedimentology*, **55**, 869-898.

Etienne, S., Mulder, T., Bez, M., Desaubliaux, G., Kwasniewski, A., Parize, O., Dujoncquoy, E. and **Salles, T.** (2012). Multiple scale characterization of sand-rich distal lobe deposit variability: Examples from the Annot Sandstones Formation, Eocene–Oligocene, SE France. *Sed. Geol*., *273*, 274, 1-18.

Fernandez, R.L., Cantelli, A., Pirmez, C., Sequeiros, O. and **Parker, G.** (2014). Growth patterns of subaqueous depositional channel lobe systems developed over a basement with a down-dip break in slope: Laboratory experiments. J. Sed. Res., **84**, 168-182.

Flint, S.S., Hodgson, D.M., Sprague, A.R., Brunt, R.L., van der Merwe, W.C., Figueiredo, J., Prélat, A., Box, D., Di Celma, C. and **Kavanagh, J.P.** (2011). Depositional architecture and sequence stratigraphy of the Karoo basin floor to shelf edge succession, Laingsburg depocentre, South Africa. *Mar. Petrol. Geol*., 28, 658-674.

Gamberi, F. and **Rovere, M.** (2011). Architecture of a modern transient slope fan (Villafranca fan, Gioia basin–Southeastern Tyrrhenian Sea). *Sed Geol*., **236**, 211-225.

Ganti, V., Lamb, M.P. and **McElroy, B.** (2014). Quantitative bounds on morphodynamics and implications for reading the sedimentary record. *Nature Comm*., **5**, Article number: 3298

Garcia, M.H. (2008) Sedimentation engineering; processes, measurements, modeling, and practice. *ASCE Manuals and reports on engineering practice*, **110**.

Gervais, A., Savoye, B., Mulder, T. and **Gonthier, E.** (2006). Sandy modern turbidite lobes: A new insight from high resolution seismic data. *Mar. Petrol. Geol*., **23**, 485-502.

Gladstone, C., Phillips, J.C. and **Sparks, R.S.** (1998). Experiments on bidisperse, constant-volume gravity currents: propagation and sediment deposition. *Sedimentology*, **45**, 833-843.

Gray, T.E., Alexander, J. and **Leeder, M.R.** (2005). Quantifying velocity and turbulence structure in depositing sustained turbidity currents across breaks in slope. *Sedimentology*, **52**, 467-488.

Grundvåg, S.A., Johannessen, E.P., Helland-Hansen, W. and **Plink-Björklund, P.** (2014). Depositional architecture and evolution of progradationally stacked lobe complexes in the Eocene Central Basin of Spitsbergen. *Sedimentology*, **61**, 535-569.

Hamilton, P., Gaillot, G., Strom, K., Fedele, J. and **Hoyal., D.** (2017). Linking hydraulic properties in supercritical submarine distributary channels to depositional-lobe geometry. *J. Sed. Res*., **87**, 935-950.

Hodgson, D.M., Flint, S.S., Hodgetts, D., Drinkwater, N.J., Johannessen, E.P. and **Luthi, S.** (2006). Stratigraphic evolution of fine-grained submarine fan systems, Tanqua depocentre, Karoo Basin, South Africa. *J. Sed. Res*., **76**, 20– 40.

Hodgson, D.M., Kane, I.A., Flint, S.S., Brunt, R.L. and **Ortiz-Karpf, A**. (2016). Time-transgressive confinement on the slope and the progradation of basin-floor fans: Implications for the sequence stratigraphy of deep-water deposits. *J. Sed. Res*., **86**, 73-86.

Jegou, I., Savoye, B., Pirmez, C. and **Droz, L.** (2008). Channel-mouth lobe complex of the recent Amazon fan: The missing piece. *Mar. Geol*., **252**, 62–77.

Johnson, S.D., Flint, S.S., Hinds, D. and **Wickens, H.d.V.** (2001). Anatomy of basin floor to slope turbidite systems, Tanqua Karoo, South Africa: sedimentology, sequence stratigraphy and implications for subsurface prediction. *Sedimentology*, **48**, 987–1023.

Kane, I.A., Pontén, A.S.M., Vangdal, B., Eggenhuisen, J.T., Hodgson, D.M. and **Spychala, Y.T.** (2017). The stratigraphic record and processes of turbidity current transformation across deep-marine lobes. *Sedimentology*, **64**, 1236–1273

Kneller, B.C. and **Branney, M.J.** (1995). Sustained high-density turbidity currents and the deposition of thick massive sands. *Sedimentology*, **42**, 607-616.

Kneller, B. and **Buckee, C.** (2000). The structure and fluid mechnics of turbidity currents: some recent studies and their geological implications. *Sedimentology*, **47**, 62-94.

Kneller, B. (2003). The influence of flow parameters on turbidite slope channel architecture. *Mar. Petrol. Geol*., **20**, 901-910.

Khripounoff, A., Vangriesheim, A., Babonneau, N., Crassous, P., Dennielou, B. and **Savoye, B.** (2003). Direct observation of intense turbidity current activity in the Zaire submarine valley at 4000 m water depth. *Mar. Geol*., **194**, 151–158. 2003

Lamb, M.P., McElroy, B., Kopriva, B., Shaw, J. and **Mohrig, D.** (2010). Linking river-flood dynamics to hyperpycnal-plume deposits: Experiments, theory, and geological implications. *Geol. Soc. Am. Bull*., **122**, 1389-1400.

Laval, A., Cremer, M., Beghin, P. and **Ravenne, C.** (1988). Density surges: two-dimensional experiment. *Sedimentology,* **35**, 73-84.

Liu, J.T., Wang, Y.-H., Yang, R.T., Hsu, R.T., Kao, S.-J., Lin, H.-L. and **Kuo, F.H.** (2012). Cyclone induced hyperpycnal turbidity currents in a submarine canyon. *J. Geophys. Res*., **117**, C04033.

Lowe, D.R. (1982). Sediment gravity flows: II. Depositional models with special reference to the deposits of high-density turbidity currents. *J. Sed. Petrol*., **52**, 279-297.

Luthi, S. (1981). Experiments on non-channelized turbidity currents and their deposits. *Mar. Geol*., **40**, M59-M68.

Marini, M., Salvatore, M., Ravnås, R. and **Moscatelli, M.** (2015). A comparative study of confined vs. semi-confined turbidite lobes from the Lower Messinian Laga Basin (Central Apennines, Italy): Implications for assessment of reservoir architecture. *Mar. Petrol. Geol*., **63**, 142-165.

McArthur, A.D., Gamberi, F., Kneller, B.C., Wakefield, M.I., Souza, P.A. and **Kuchle, J.** (2017). Palynofacies classification of submarine fan depositional

772 environments: Outcrop examples from the Marnoso-Arenacea Formation, Italy. *Mar.*
773 *Petrol. Geol.*, **88**, 181-199.
774
775 **Middleton, G.V.** and **Hampton, M.A.** (1973). Part I. Sediment gravity flows:
776 Mechanics of flow and deposition. Pacific Section SEPM, 1-38.
777
778 **Morris, E.A., Hodgson, D.M., Flint, S.S., Brunt, R.L., Butterworth, P.L.** and
779 **Verhaeghe, J.** (2014). Sedimentology, stratigraphic architecture and depositional
780 context of submarine frontal lobe complexes. *J. Sed. Res*., **84**, 763-780.
781
782 **Mulder, T.** and **Alexander, J.** (2001). Abrupt change in slope causes variation in the
783 deposit thickness of concentrated particle-driven density currents. *Mar. Geol*., **175**,
784 221-235.
785
786 **Mulder, T.** and **Etienne, S.** (2010). Lobes in deep-sea turbidite systems: State of the
787 art. *Sed. Geol*., **229**, 75-80.
788
789 **Mutti, E.** (1977). Distinctive thin-bedded turbidite facies and related depositional
790 environments in the Eocene Hecho Group (South-central Pyrenees, Spain).
791 *Sedimentology*, **24**, 107-131.
792
793 **Mutti, E.** (1992). Turbidite Sandstones, Agip -Instituto di Geologia, Università di
794 Parma, Italy, 275p.
795

Mutti, E. and **Normark, W.R.** (1987). Comparing examples of modern and ancient turbidite systems: Problems and concepts. In: Marine Clastic Sedimentology: Concepts and Case Studies (Eds. J.K. Leggett and C.G. Zuffa) Graham & Trotman, London, 1-38.

Nelson, C.H., Twichell, D.C., Schwab, W.C., Lee, H.J. and **Kenyon, N.H.** (1992). Upper Pleistocene turbidite sand beds and chaotic silt beds in the channelized, distal, outer-fan lobes of the Mississippi fan. *Geology*, **20**, 693–696.

Normark, W.R. (1970). Channel piracy on Monterey Deep-Sea Fan. Deep-Sea. Deep-Sea Research and Oceanographic Abstracts 17, 837-846.

Normark, W.R. (1978). Fan valleys, channels, and depositional lobes on modern submarine fans: Characters for recognition of sandy turbidite environments. *AAPG Bull.*, **62**, 912-931.

Ouchi, S., Ethridge, F.G., James, E.W. and **Schumm, S.A.** (1995). Experimental study of subaueous fan development. In: Hartley, A.J., Prosser, D.J. (Eds.), Characterization of Deep Marine Clastic Systems. *Geol. Soc. Spec. Publ*., **4**, 13-29.

Palanques, A., Kenyon, N.H., Aloso, B. and **Limonov, A.** (1995). Erosional and depositional patterns in the Valencia Channel mouth: An example of a modern channel-lobe transition zone. *Mar. Geophys. Res*., **17**, 503-517.

Parsons, J.D., Schweller, W.J., Stelting, C.W., Southard, J.B., Lyons, W.J. and **Grotzinger, J.P.** (2002). A preliminary experimental study of turbidite fan deposits. *J. Sed. Res*., **72**, 619-628.

Pirmez, C., Prather, B.E., Mallarino, G., O'Hayer, W.W., Droxler, A.W. and **Winker, C.D.** (2012). Chronostratigraphy of the Brazos-Trinity depositional system, Western Gulf of Mexico: Implications for deepwater depositional models. In: *Application of the Principles of Seismic Geomorphology to Continental -Slope and Base-of-Slope Systems: Case Studies from Seafloor and Near-Seafloor Analogues* (Eds. B.E. Prather, M.E. Deptuck, D. Mohrig, B. van Hoorn and R.B. Wynn). *SEPM Spec. Publ.*, **99**, 112- 143.

Porten, K.W., Kane, I.A., Warchoł, M.J. and **Southern, S.J.** (2017). A sedimentological process-based approach to depositional reservoir quality of deep-marine sandstones: an example from the Springar Formation, north-western Vøring Basin, Norwegian Sea. *J. Sed. Res*., **86**, 1269-1286.

Posamentier, H.W. and **Kolla, V.** (2003). Seismic geomorphology and stratigaphy of depositional elements in deep-water settings. *J. Sed. Res.*, **73**, 367-388.

Pohl, F., Eggenhuisen, J.,Cartigny, M.,Tilston, M., de Leeuw, J. and **Hermidas, N. (2019a).** The Influence of a Slope Break on Turbidite Deposits: An Experimental Investigation. *EarthArXiv*. June 24. doi:10.31223/osf.io/v58gm

Prather, B.E., Booth, J.R., Steffens, G.S. and **Craig, P.A.** (1998). Classification, lithologic calibration, and stratigraphic succession of seismic facies of intraslope basins, Deep-Water Gulf of Mexico. *AAPG Bull.,* **82**, 701-728.

Prélat, A., Hodgson, D.M. and Flint, S.S. (2009). Evolution, architecture and hierarchy of distributary deep-water deposits: a high-resolution outcrop investigation from the Permian Karoo Basin, South Africa. *Sedimentology*, **56**, 2132-2154.

Prélat, A., Covault, J.A., Hodgson, D.M., Fildani, A. and **Flint, S. S.** (2010). Intrinsic controls on the range of volumes, morphologies, and dimensions of submarine lobes. *Sed. Geol*., **232**, 66-76.

Prélat, A. and **Hodgson, D.M.** (2013). The full range of turbidite bed thickness patterns in submarine lobes: controls and implications. *J. Geol. Soc. London*, **170**, 1-6.

Pyles, D.R., Straub, K.M. and **Stammer, J.G.** (2013). Spatial variations in the composition of turbidites due to hydrodynamic fractionation. *Geophys. Res. Lett*., **40**, 3919-3923.

Richardson, J.F. and **Zaki, W.N.** (1954). The sedimentation of a suspension of uniform spheres under conditions of viscous flow. *Chem. Eng. Sci*., **3**, 65-73.

Romans, B.W., Castelltort, S., Covault, J.A., Fildani, A. and **Walsh, J.P.** (2016). Environmental signal propagation in sedimentary systems across timescales. *Earth-Science Reviews,* **153**, 7-29.

Saller, A.H., Noah, J.T., Prama Ruzuar, A. and **Schneider, R.** (2004). Linked lowstand delta to basin-floor fan deposition, offshore Indonesia: An analog for deep-water reservoir systems. *AAPG Bull*., **88**, 21-46.

Saller, A., Werner, K., Sugiaman, F., Cebastiant, A., May, R., Glenn, D. and **Barker, C.** (2008). Characteristics of Pleistocene deep-water fan lobes and their application to an upper Miocene reservoir model, offshore East Kalimantan, Indonesia. *AAPG Bull*., **92**, 919–949.

Satur, N., Hurst, A., Cronin, B.T., Kelling, G. and **Gürbüz, K.** (2000). Sand body geometry in a sand-rich, deep-water clastic system, Miocene Cingöz Formation of southern Turkey. *Mar. Petrol. Geol*., **17**, 239-252.

Sohn, Y.K. (1997). On traction-carpet sedimentation. *J. Sed. Geol*., **67**, 502-509.

Southard, J.B. and **Mackintosh, M.E.** (1981). Experimental test of autosuspension. *Earth Surf. Proc. Land*., **6**, 103-111.

Spychala, Y.T., Hodgson, D.M., Prélat, A., Kane, I.A., Flint, S.S. and **Mountney, N.P.** (2017a). Frontal and Lateral Submarine Lobe Fringes: Comparing Sedimentary Facies, Architecture and Flow Processes. *J. Sed. Res.*, **87**, 75-96.

Spychala, Y.T., Hodgson, D.M., Stevenson, C.J. and **Flint, S.S.** (2017b). Aggradational lobe fringes: The influence of subtle intrabasinal seabed topography on

sediment gravity flow processes and lobe stacking patterns. *Sedimentology*, **64**, 582–608.

Steel, E., Buttles, J., Simms, A.R., Mohrig, D., and **Meiburg, E.** (2017). The role of buoyancy reversal in turbidite deposition and submarine fan geometry. *Geology*, **45**, 35-38.

Stevenson, C.J., Jackson, C.A-L., Hodgson, D.M., Hubbard, S.M. and **Eggenhuisen, J.T.** (2015) Sediment bypass in deep-water systems from modern seafloor, outcrop, subsurface and experimental data. *J. Sed. Res*., **85**, 1058-1081.

Stevenson, C.J., Feldens, P., Georgiopoulou, A., Schönke, M., Krastel., S., Piper, D.J.W., Lidhorst, K. and **Mosher, D.** (2018). Reconstructing the sediment concentration of a giant submarine gravity flow. *Nature Comm*., **9**, Article number: 2616.

Straub, K.M. and **Pyles, D. R.** (2012). Quantifying the Hierarchical Organization of Compensation In Submarine Fans Using Surface Statistics. *J. Sed. Res.,* **82**, 889-898.

Talling, P.J., Paill, C.K. and **Piper, D.J.W.** (2013). How are subaqueous sediment density flows triggered, what is their internal structure and how does it evolve? Direct observations from monitoring of active flows. *Earth-Sci. Rev*., **125**, 244-287.

Tilston, M., Arnott, R.W.C., Rennie, C.D. and **Long, B.** (2015). The influence of grain size on the velocity and sediment concentration profiles and depositional record of turbidity currents. *Geology*, **43**, 839-842.

Twichell, D.C., Schwab, W.C., Nelson, C.H., Kenyon, N.H. and **Lee, H.J.** (1992). Characteristics of a sandy depositional lobe on the outer Mississippi fan from DeaMARC IA sidescan sonar images. *Geology*, **20**, 689–692.

van der Werff, W. and **Johnson, S.** (2003). High resolution stratigraphic analysis of a turbidite system, Tanqua Karoo Basin, South Africa: *Mar. Petrol. Geol*., **20**, 45-69.

Wynn, R.B., Weaver, P.E., Masson, D.G. and **Stow, D.A.V.** (2002). Turbidite depositional architecture across three interconnected deep-water basins on the north-west African margin. *Sedimentology*, **49**, 669-695.

Xu, J.P., Sequeiros, O.E. and **Noble, M.A.** (2014). Sediment concentrations, flow conditions, and downstream evolution of two turbidity currents, Monterey Canyon, USA. Deep-Sea Research I 89, 11-34.

FIGURE CAPTIONS

Figure 1: Width vs length values for lobes deposited in the Karoo Basin (Prélat et al., 2009), the Amazon Fan (Jegou et al., 2008), the Golo Fan (Deptuck et al., 2008), the Kutai Basin (Saller et al., 2008), the Giza Field (Morris et al., 2014) and the Al Batha Turbidite System (Bourget et al., 2010) and their length:width aspect ratios.

Figure 2: A) The experimental set-up consists of three areas: 1) slope with a 11° gradient with a pre-formed channel, 2) basin floor with varying gradient (0-4°), and 3)

horizontal plain which is used to install the UVP probes. B) Set-up of UVP probes in relation to the pre-formed channel. Four UVPs probes are located longitudinal to the channel form. Probe numbers are marked in white.

Figure 3: Schematic of an experimental deposit and the measured parameters.

Figure 4: Erosion/deposition maps of Series I (basin floor angle). Blue colours represent deposition, red colours erosion. As the basin floor becomes steeper (A to E) the deposit becomes more elongated and the depocenter is relocated further basinwards. Erosional patterns in front of the inlet are an experimental artefact.

Figure 5: Topographic profiles showing the longitudinal geometry of the deposits. A: Run 1 shows the highest thickness of 8.8 cm 1m from the break of slope. The deposit thins subsequently as the basin floor angle increases and the point of maximum thickness shifts farther into the basin. Run 6 for example has a thickness of 6.2 cm 2.7 m from the break of slope. B: Runs with varying concentrations produce two types of geometries. The higher concentration runs (Run 5 and 6) have deposits that reach far into the basin and show their maximum thickness at 3.0 and 2.7 m from the break of slope, respectively, whereas lower concentration runs (Run 7 and 8) have wedge-shaped longitudinal geometries with their maximum thickness directly after the break of slope. C: Runs with different discharges produce similar geometries. However, the onlap of the deposit produced by Run 9 (lowest discharge) is significantly upstream of the break of slope (also see Fig. 10), while Run 10 (highest discharge) produces an area of low sedimentation behind the break of slope. The deposit starts thickening 1.0 m into the basin.

968

969 Figure 6: Surface area over distance from the break of slope a proxy of volume
970 distribution. A: Distributions for Series I imply that steeper basin-floor angles are more
971 efficient in transporting sediment resulting in a basinward relocation of the depocentre.
972 B: Distributions for Series II show that higher concentration currents will deposit the
973 bulk volume of sediment farther in the basin, while lower concentration currents
974 aggrade deposits in front of the break of slope and taper downstream. C: Distributions
975 for Series III display that higher discharges will result in more basinward located
976 depocentres, wheres lower discharges will shift the depocentre upstream.

977

978 Figure 7: Erosion/deposition maps of Series II (changing sediment volume
979 concentration). Deposits from currents with lower sediment concentration are shorter.

980

981 Figure 8: Cross-section view for different distances behind the break of slope. A: Run
982 6 shows an indent into its convex up shape near the break of slope indicating increased
983 bypass of the current. B: Convex up shaped geometry of Run 7.

984

985 Figure 9: Digital elevation models (DEMs) of the deposits created by changing
986 discharge. A: The deposit of Run 9 (lowest discharge) onlaps high onto the slope. B:
987 The deposits of Run 6 (medium discharge) onlaps at the base of slope. C: The deposit
988 of Run 10 (highest discharge) is detached from the slope by an area of low deposition.

989

990 Figure 10: Maximum velocity and flow height graphs for Series I (A), Series II (B) and
991 Series III (C).

992

Figure 11: A: Diagram of lobe hierarchy dependent compensation; B: Planview relationship between lobe elements forming a lobe. Yellow colours mark sand-prone deposits, grey colours silt-prone deposits (modified from Straub et al., 2012).

Figure 12: Measured lobe element length versus calculated advection lobe element length. Generally, calculated lengths are around 75 % accurate. This means that advection length can be used as a first order estimation of lobe element length, although length values are consistently under predicted.

Figure 13: Limitations of the advection length scale approach. A: The method is highly dependent on the input of average grain size. All grain sizes below the d50 are omitted from the length estimation. B: In runs with high concentration and high discharge the depocentre is shifted farther basinwards. The calculated length of the deposit of Run 10 does not only underestimate the length dimensions, but would also omit the main depocentre of the depositional body.

Figure 14: Simplified lobe model showing sand-prone, heterolithic and silt-prone dominated environments. The sandy lobe only represents a small part of the full lobe. A: In planview the silt-prone deposits surround the sandy lobe like a halo. B: Longitudinal cross-section shows that siltstone deposits form an extensive thin layer into the basin.

Table 1: Overview of the experimental parameters for the ten conducted runs.

Table 2: Summary of maximum dimensions and aspect-ratios for the deposits of all conducted runs.

Table 3: Values used to calculate lobe element length. Flow velocity (u, in m/s), flow height (h, in m), settling height (h, in m), settling velocity (w_s, in m/s), and advection length (l_a, in m) .

Table 4: Reconstructed turbidity current velocities from include the Amazon Fan (Jegou et al., 2008), Fan 3, Tanqua depocentre, Karoo Basin (Prélat et al., 2009, Kane et al., 2017), the Golo Fan offshore Corsica (Deptuck et al., 2008, Hamilton et al., 2017) and the Pleistocene Fan, Kutai Basin, Indonesia (Saller et al., 2004, 2008)

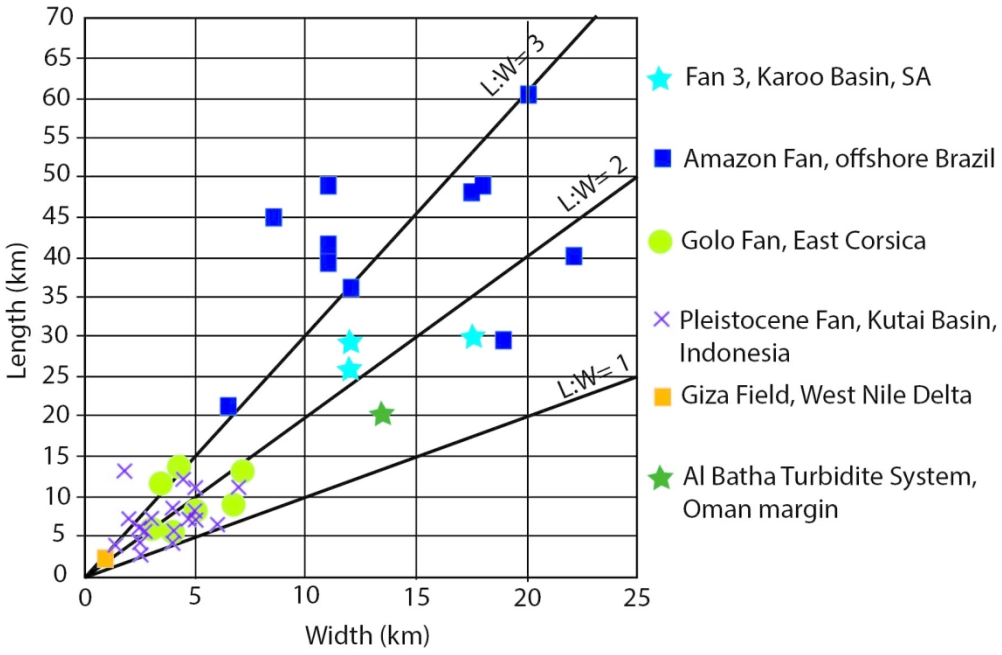

Figure 1

155x100mm (300 x 300 DPI)

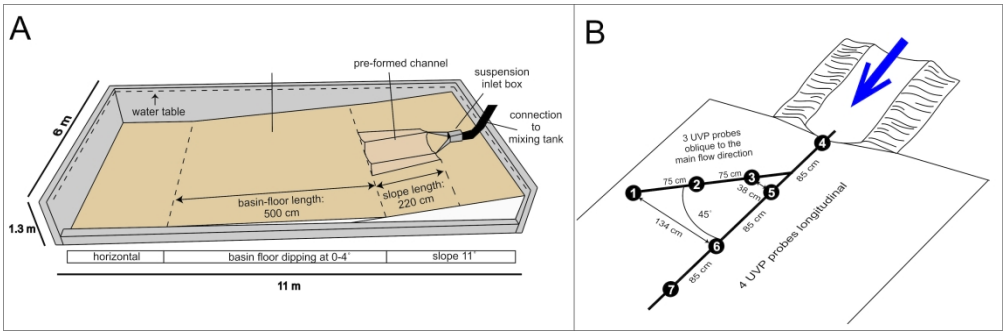

Figure 2

391x127mm (300 x 300 DPI)

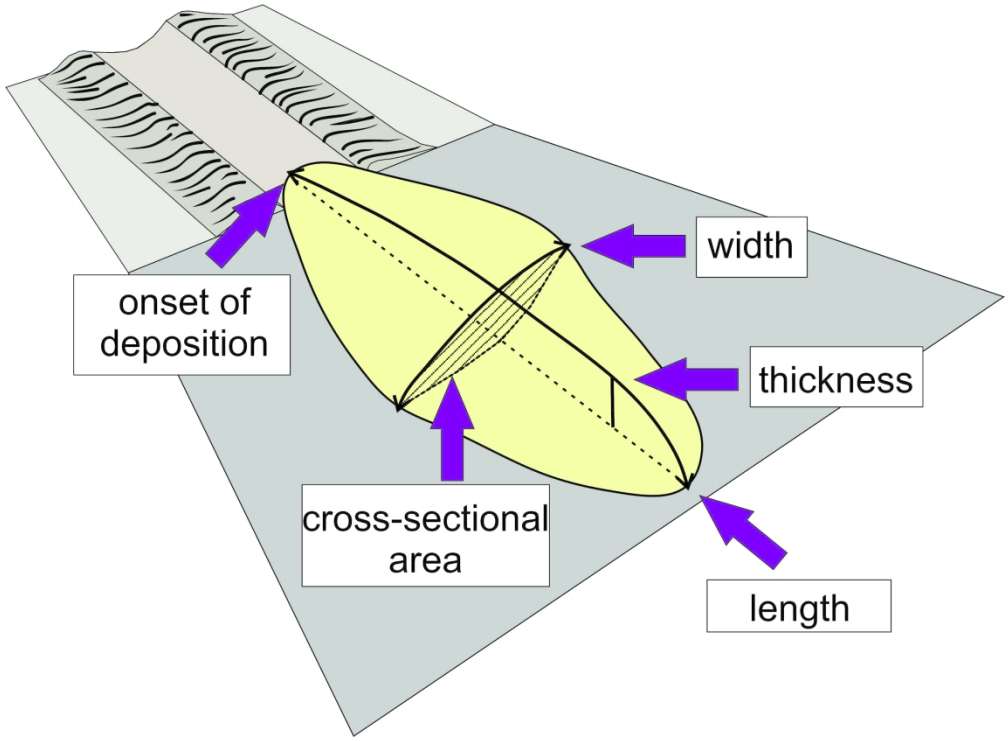

Figure 3

228x167mm (300 x 300 DPI)

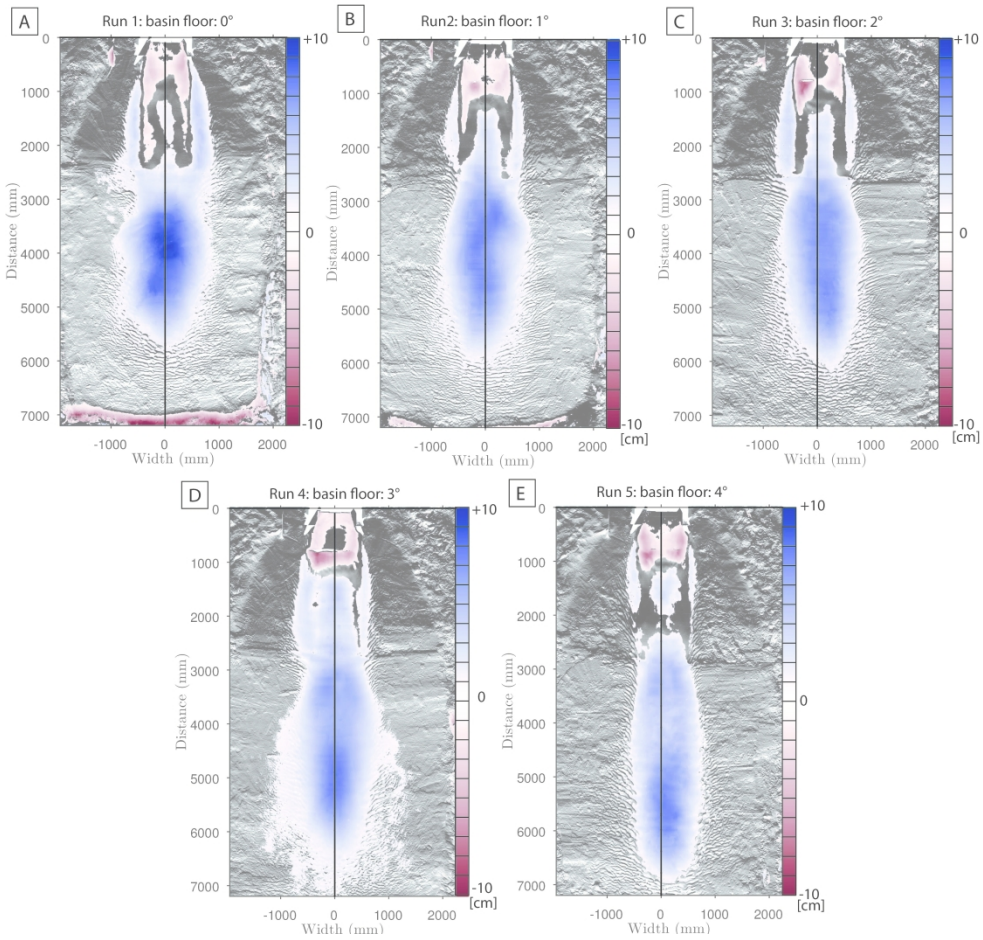

Figure 4

1139x1073mm (96 x 96 DPI)

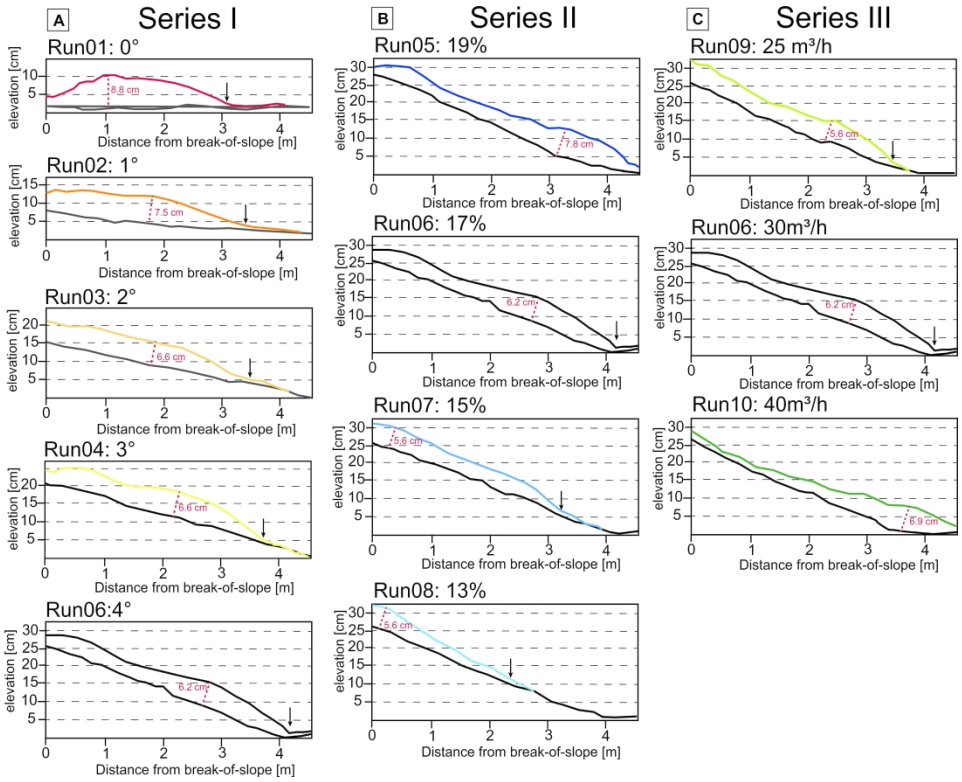

Figure 5

448x345mm (300 x 300 DPI)

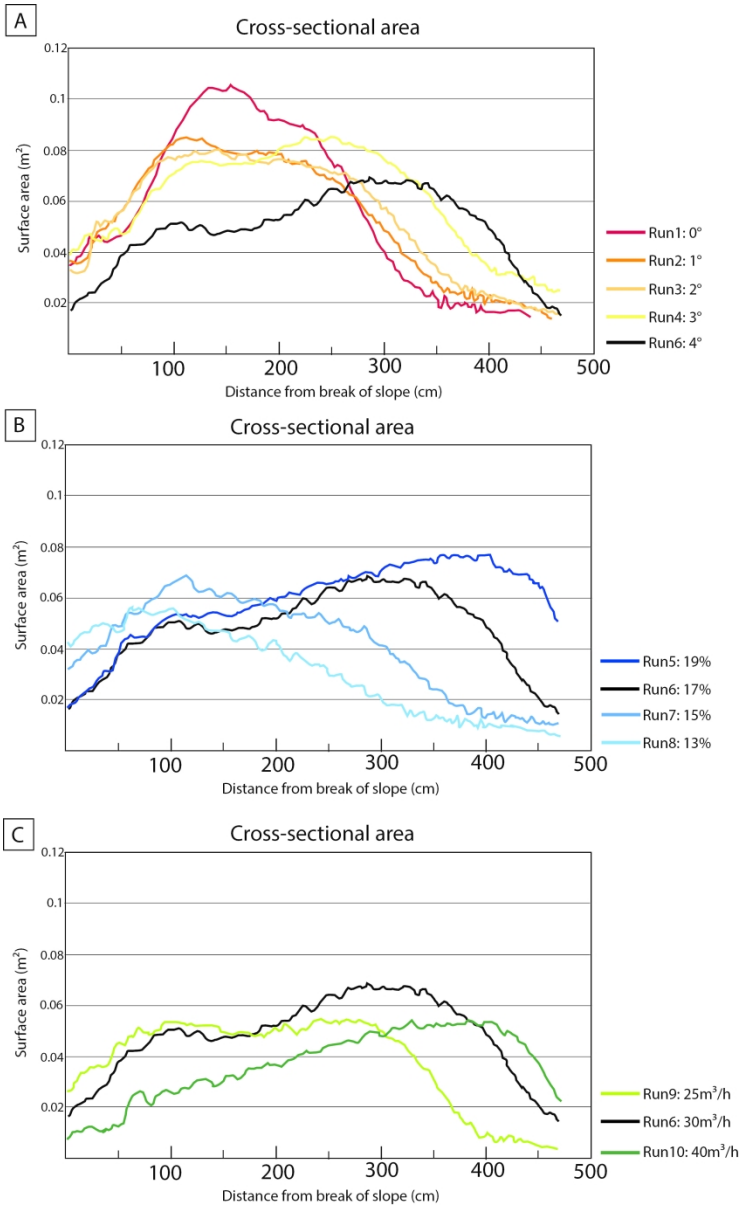

Figure 6

233x379mm (300 x 300 DPI)

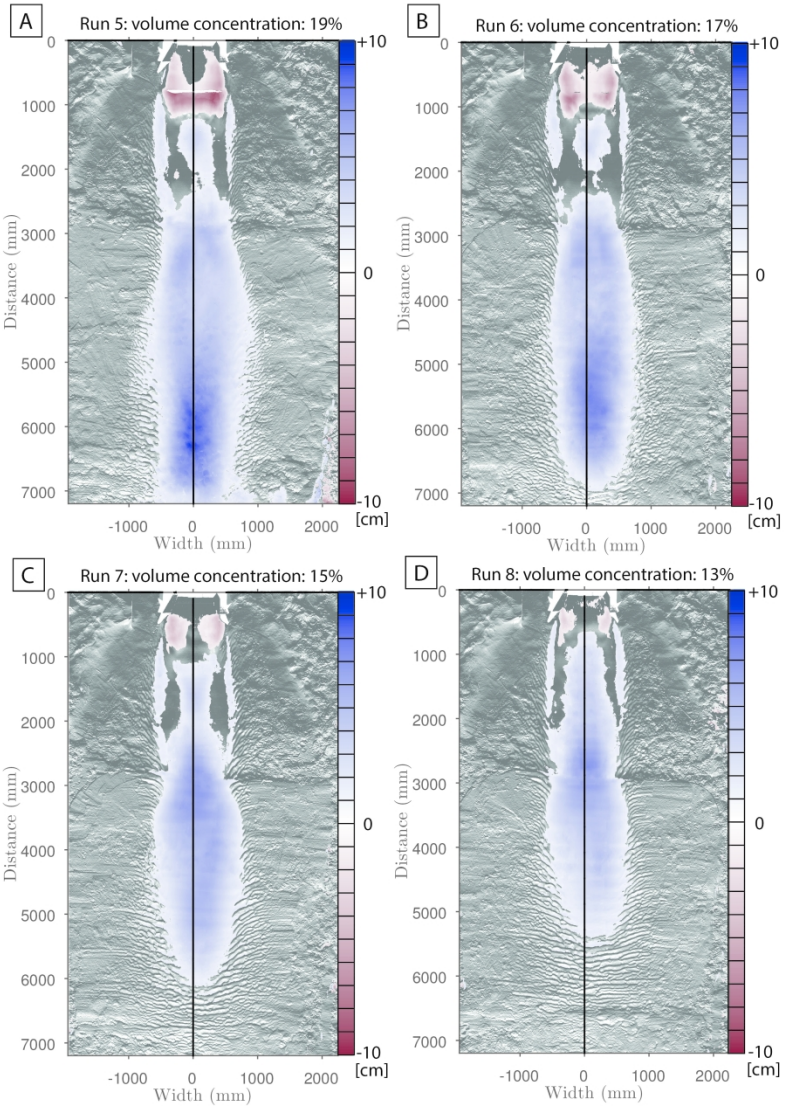

Figure 7

297x366mm (300 x 300 DPI)

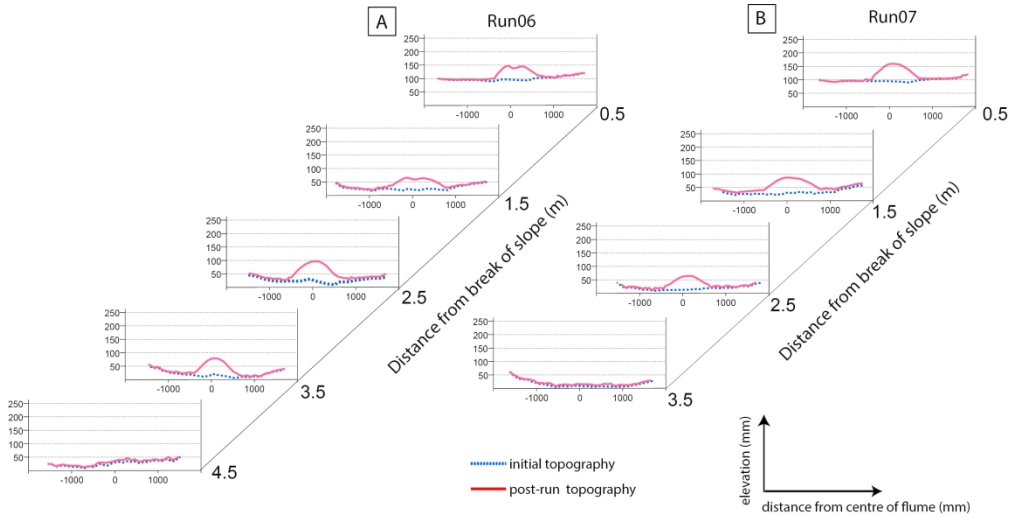

Figure 8

348x178mm (300 x 300 DPI)

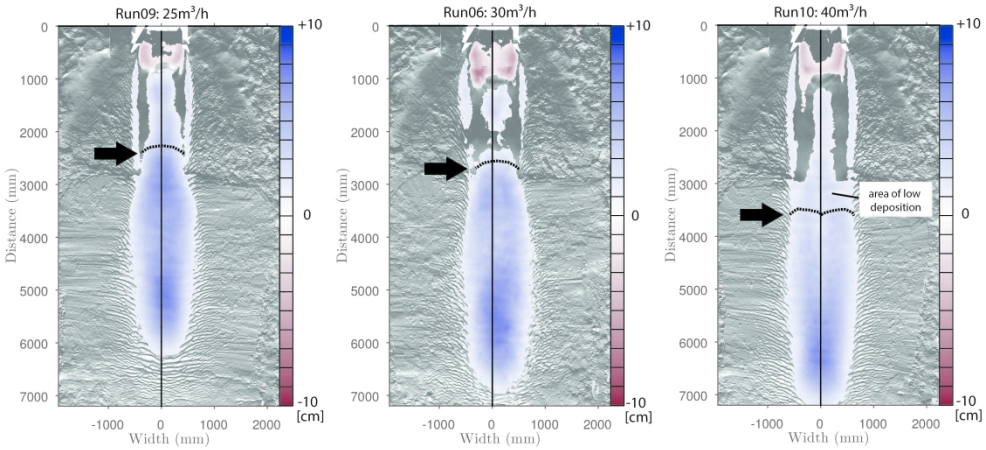

Figure 9

371x172mm (300 x 300 DPI)

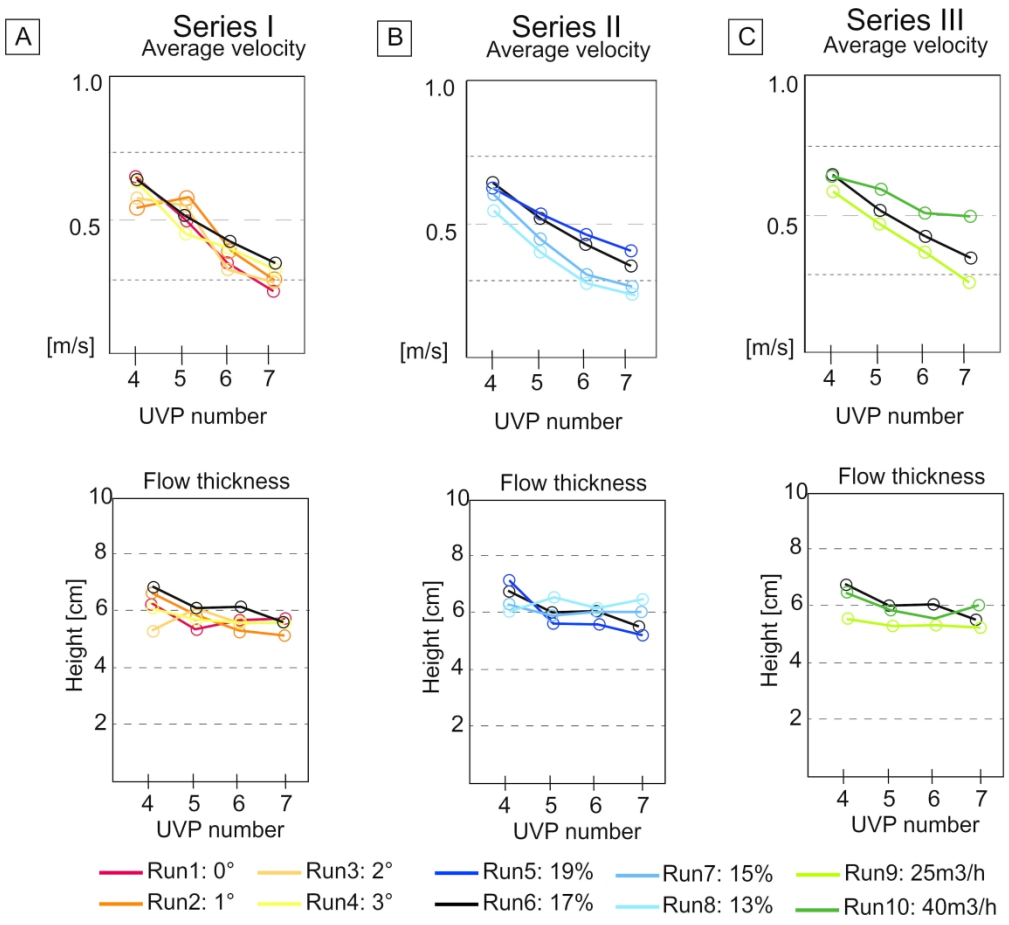

Figure 10

282x256mm (300 x 300 DPI)

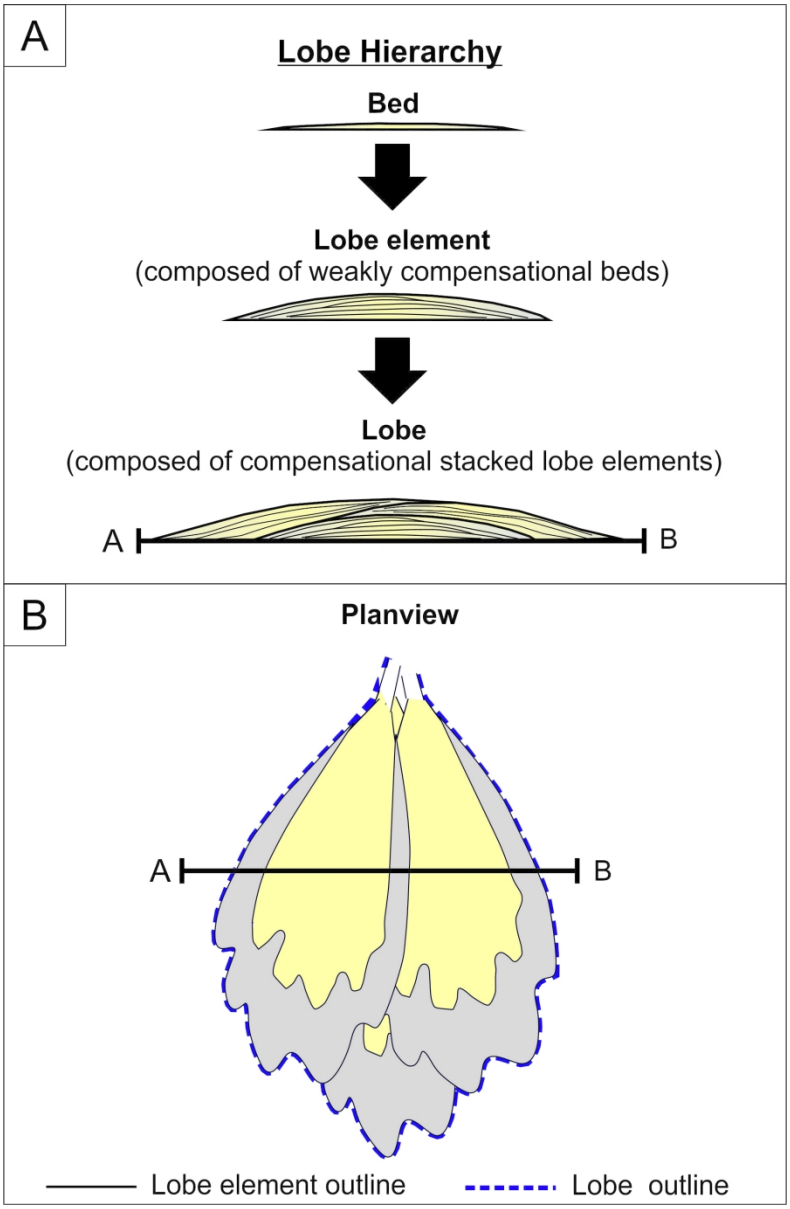

Figure 11

161x246mm (300 x 300 DPI)

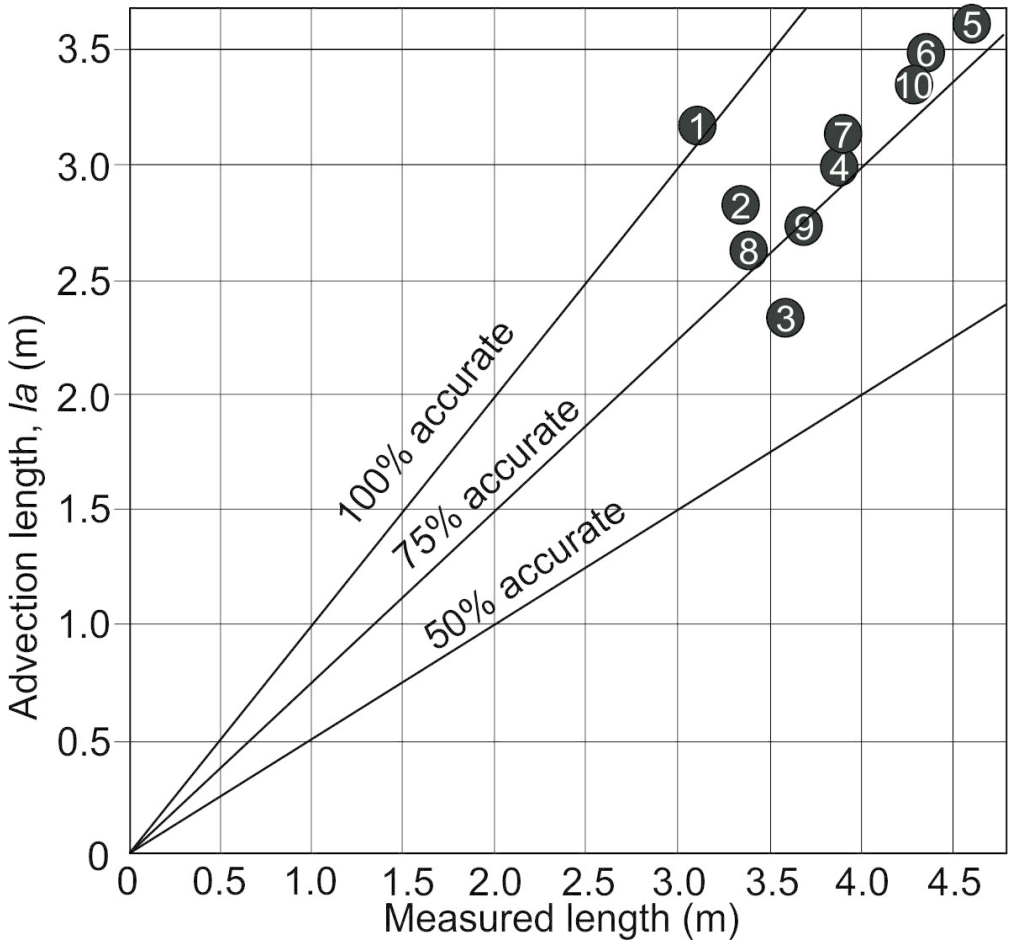

Figure 12

100x94mm (300 x 300 DPI)

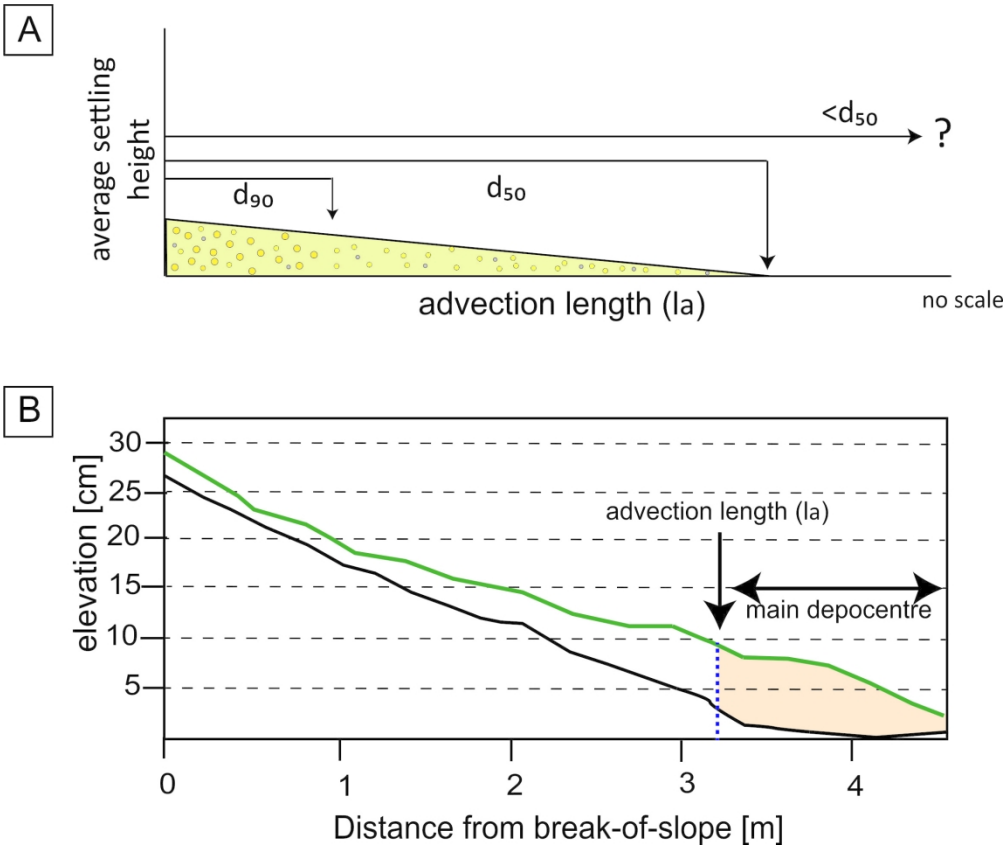

Figure 13

197x166mm (300 x 300 DPI)

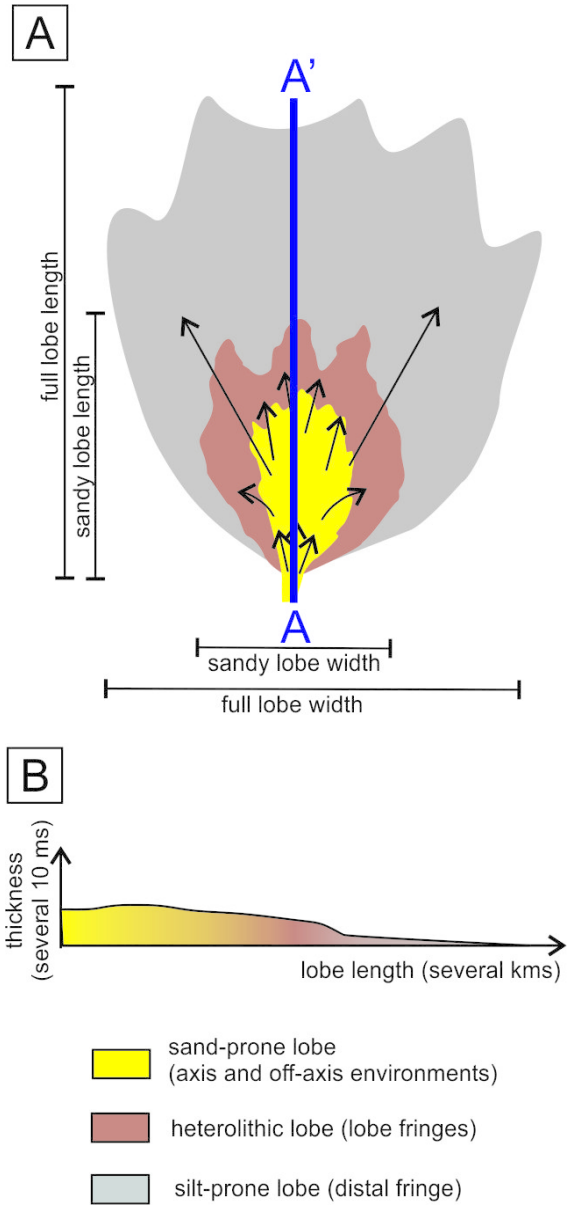

Figure 14

54x115mm (300 x 300 DPI)

Series	Run number	slope angle (°)	basin-floor angle (°)
1	1	11	0
1	2	11	1
1	3	11	2
1	4	11	3
2	5	11	4
1,2,3	6	11	4
2	7	11	4
2	8	11	4
3	9	11	4
3	10	11	4

concentration (Vol%)	discharge m3/h
17	30
17	30
17	30
17	30
19	30
17	30
15	30
13	30
17	25
17	40

Series	Run#	max thickness (cm)	max length (cm)	max width (cm)	L/W
1	1	8.8	310	186	1.7
1	2	7.5	335	181.5	1.8
1	3	6.6	357	152	2.3
1	4	6.6	383	156	2.5
2	5	7.8	465	138.5	3.4
1,2,3	6	6.2	444	143	3.1
2	7	5.6	390	143	2.7
2	8	5.6	340	123	2.8
3	9	5.6	370	117.5	3.1
3	10	6.9	430	126.5	3.4

W/T	L/T	channel length after run
21.1	35.2	225
24.2	44.7	216
23.0	54.1	207
23.6	58.0	214
17.8	59.6	204
23.1	71.6	210
25.5	69.6	206
22.0	60.7	200
21.0	66.1	190
18.3	62.3	250

Run #	u (m/s)	w_s (m/s)	h (m)	l_a (m)	measured length (m)	accuracy (%)
1	0.64	0.0123	0.061	3.2	3.10	102
2	0.53	0.0123	0.065	2.8	3.35	84
3	0.56	0.0123	0.053	2.4	3.57	68
4	0.62	0.0123	0.060	3.0	3.83	79
5	0.62	0.0123	0.071	3.6	4.65	77
6	0.63	0.0123	0.068	3.5	4.44	78
7	0.61	0.0123	0.062	3.1	3.90	79
8	0.54	0.0123	0.060	2.6	3.40	77
9	0.59	0.0123	0.057	2.7	3.70	74
10	0.65	0.0123	0.064	3.4	4.30	79

study area	length(m)	average grain size (m)	ws (m/s)
Fan3, Tanqua , Karoo	26000	0.000125	0.011
lobe	30000	0.000125	0.011
	29500	0.000125	0.011
Amazon fan	40000	0.000094	0.0068
lobe	39000	0.000094	0.0068
	48000	0.000094	0.0068
	21000	0.000094	0.0068
	41000	0.000094	0.0068
	60500	0.000094	0.0068
	49000	0.000094	0.0068
	49000	0.000094	0.0068
	29500	0.000094	0.0068
	45000	0.000094	0.0068
	36000	0.000094	0.0068
Golo fan, East Corsica	6500	0.0025	0.0318
lobe	5800	0.0025	0.0318
	6000	0.0025	0.0318
	5700	0.0025	0.0318
	8200	0.0025	0.0318
	6000	0.0025	0.0318
	11800	0.0025	0.0318
	14000	0.0025	0.0318
	12500	0.0025	0.0318
	8800	0.0025	0.0318
	13500	0.0025	0.0318
Indonesia, Kutai Basin	7000	0.000187	0.021
lobe	5600	0.000187	0.021
	8000	0.000187	0.021
	2500	0.000187	0.021
	6400	0.000187	0.021
	7000	0.000187	0.021
	11000	0.000187	0.021
	7000	0.000187	0.021
	11000	0.000187	0.021
	13000	0.000187	0.021
	4000	0.000187	0.021
	3700	0.000187	0.021
	12000	0.000187	0.021
	8400	0.000187	0.021
	4000	0.000187	0.021
	6000	0.000187	0.021
	7000	0.000187	0.021
	5500	0.000187	0.021
Fan3, Tanqua , Karoo	5000	0.000125	0.011
lobe elment			

hs (reported channel depth; m)	calculated velocity m/s
13	22
13	25.38
13	24.96
20	13.6
20	13.26
20	16.32
20	7.14
20	13.94
20	20.57
20	16.66
20	16.66
20	10.03
20	15.3
20	12.24
14	14.76
14	13.17
14	13.63
14	12.95
14	18.63
14	13.63
14	26.80
14	31.8
14	28.39
14	19.99
14	30.66
30	4.9
30	3.92
30	5.6
30	1.75
30	4.48
30	4.9
30	7.7
30	4.9
30	7.7
30	9.1
30	2.8
30	2.59
30	8.4
30	5.88
30	2.8
30	4.2
30	4.9
30	3.85
13	4.2